



UNIVERSITY OF LEEDS

This is a repository copy of *Chemical Signatures of Melt–Rock Interaction in the Root of a Magmatic Arc*.

White Rose Research Online URL for this paper:
<http://eprints.whiterose.ac.uk/135919/>

Version: Accepted Version

Article:

Stuart, CA, Meek, U, Daczko, NR et al. (2 more authors) (2018) Chemical Signatures of Melt–Rock Interaction in the Root of a Magmatic Arc. *Journal of Petrology*, 59 (2). pp. 321-340. ISSN 0022-3530

<https://doi.org/10.1093/petrology/egy029>

(c) The Author(s) 2018. Published by Oxford University Press. All rights reserved. This is a pre-copyedited, author-produced version of an article accepted for publication in *Journal of Petrology* following peer review. The version of record is available online at:
<https://doi.org/10.1093/petrology/egy029>.

Reuse

Items deposited in White Rose Research Online are protected by copyright, with all rights reserved unless indicated otherwise. They may be downloaded and/or printed for private study, or other acts as permitted by national copyright laws. The publisher or other rights holders may allow further reproduction and re-use of the full text version. This is indicated by the licence information on the White Rose Research Online record for the item.

Takedown

If you consider content in White Rose Research Online to be in breach of UK law, please notify us by emailing eprints@whiterose.ac.uk including the URL of the record and the reason for the withdrawal request.



eprints@whiterose.ac.uk
<https://eprints.whiterose.ac.uk/>



Draft Manuscript for Review

Chemical signatures of melt–rock interaction in the root of a magmatic arc

Journal:	<i>Journal of Petrology</i>
Manuscript ID	Draft
Manuscript Type:	Original Manuscript
Date Submitted by the Author:	n/a
Complete List of Authors:	Stuart, Catherine; Macquarie University, Earth and Planetary Sciences Meek, Uvana; Macquarie University, Earth and Planetary Sciences Daczko, Nathan; Macquarie University, Earth and Planetary Sciences Piazolo, Sandra; Macquarie University, Department of Earth and Planetary Sciences Huang, Jinxiang; Macquarie University, Earth and Planetary Sciences
Keyword:	amphibolite, hydration, lower crust, melt–rock interaction, porous melt flow

SCHOLARONE™
Manuscripts

1
2
3 1 **CHEMICAL SIGNATURES OF MELT–ROCK INTERACTION IN THE**
4
5
6 2 **ROOT OF A MAGMATIC ARC**
7

8
9 3 Stuart, C.A. *, Meek, U., Daczko, N.R., Piazzolo, S., Huang, J.-X.

10
11 4 *Australian Research Council Centre of Excellence for Core to Crust Fluid Systems (CCFS)*
12
13 5 *and GEMOC, Department of Earth and Planetary Sciences, Macquarie University, Sydney,*
14
15 6 *NSW 2109, Australia*
16

17
18
19 7 Corresponding author: C. Stuart (T: +61 2 9850 4715; F: +61 2 9850 6904; E:

20
21 8 catherine.stuart@students.mq.edu.au)
22

23
24 9 Running title: Chemical signatures of melt–rock interaction
25
26
27
28
29
30
31
32
33
34
35
36
37
38
39
40
41
42
43
44
45
46
47
48
49
50
51
52
53
54
55
56
57
58
59
60

1
2
3 10 **ABSTRACT**
4
5

6 11 Identification of melt–rock interaction during melt flux through crustal rocks is limited to
7
8 12 field relationships and microstructural evidence, with little consideration given to
9
10 13 characterising geochemical signatures of this process. We examine the mineral and whole
11
12 14 rock geochemistry of four distinct styles of melt–rock interaction during melt flux through the
13
14 15 Pembroke Granulite, a gabbroic gneiss from the Fiordland magmatic arc root. Volume, spatial
15
16 16 distribution, and cumulate flux of melt, as well as P–T–X conditions and stress field vary
17
18 17 between each melt flux style. Whole rock metasomatism is not detected in three of the four
19
20 18 melt flux styles. Mineral assemblage and major element mineral composition in modified
21
22 19 rocks are dictated by P–T–X conditions, as in sub-solidus metamorphic systems.
23
24 20 Heterogeneous mineral major and trace element compositions are linked to low cumulate
25
26 21 volumes of melt flux, which inhibits widespread modification and equilibration. Amphibole
27
28 22 and clinozoisite in modified rocks have igneous-like REE patterns, formed by growth and/or
29
30 23 recrystallisation in the presence of melt and large equilibration volumes provided by the grain
31
32 24 boundary network of melt. Heterogeneities in mineral REE compositions are linked to
33
34 25 localisation of melt flux by deformation and resulting smaller equilibration volumes, and/or
35
36 26 variation in the composition of the fluxing melt. The presence of igneous-like mineral REE
37
38 27 chemical signatures in a metamorphic rock, combined with microstructural evidence for the
39
40 28 former presence of melt, are proposed as powerful indicators of melt–rock interaction during
41
42 29 melt flux.
43
44
45
46
47

48 30 **Key words:** amphibolite; hydration; lower crust; melt–rock interaction; porous melt flow
49
50
51
52
53
54
55
56
57
58
59
60

31 INTRODUCTION

32 Partial melting, melt migration and crystallisation are fundamental processes responsible for
33 the chemical evolution of the Earth's crust. Each process imparts a different geochemical
34 signature on the melt and surrounding rock with which it reacts. Despite demonstrations that
35 melt–rock interaction during melt migration produces distinctive chemical signatures in the
36 mantle (e.g. Lundstrom *et al.*, 1995, Nicolas, 1986, Pirard & Hermann, 2015, Rampone *et al.*,
37 1994, Spiegelman & Elliott, 1993), little consideration is given to geochemical signatures
38 produced by melt–rock interaction during melt migration in the crust.

39 Melt–rock interaction in crustal rocks is rarely documented due to the inherent
40 complexity of crustal rock types and melt compositions, and a lack of criteria for
41 identification of the former flux of melt. Evidence for melt–rock interaction in the field may
42 take the form of distributed or narrow zones of modification, such as hydration (e.g. Daczko
43 *et al.*, 2002b, Stuart *et al.*, in press), or bodies of rock with igneous features that lack intrusive
44 or structural boundaries with adjacent metamorphic rock (e.g. Daczko *et al.*, 2016). The most
45 robust indicator is observation of microstructures indicative of the former presence of melt
46 (e.g. Holness, 2008, Sawyer, 1999, Vernon, 2011, White *et al.*, 2005) in rocks where in situ
47 partial melting reactions are not interpreted. Microstructures indicative of a replacement
48 reaction are also common in the deep crust, especially in rocks partially modified by flux of
49 an externally-derived melt (Stuart *et al.*, in press, Stuart *et al.*, 2016). Though physical
50 indicators of the former presence of melt are identified via comparison with igneous rocks and
51 migmatites, little attention has been given to establishing geochemical signatures indicative of
52 melt–rock interaction.

53 Geochemical signatures in exposed arc roots and plutons are widely used to infer
54 metamorphic and igneous processes occurring at depth. For example, studies have shown that

1
2
3 55 metamorphic reactions in the lower crust do not necessarily mobilise rare earth elements
4
5 56 (REE) over large distances, due to slow diffusion rates (e.g. Cherniak, 2003, Chernoff &
6
7 57 Carlson, 1999, Tirone *et al.*, 2005, Van Orman *et al.*, 2001) and poor partitioning into
8
9 58 aqueous fluids (Cullers & Graf, 1984, Cullers *et al.*, 1973, Flynn & Burnham, 1978,
10
11 59 Wendlandt & Harrison, 1979). As a result, metamorphic products in sub-solidus or fluid-poor
12
13 60 conditions (e.g. Daczko *et al.*, 2009) may inherit their chemical signatures from reactant
14
15 61 minerals (e.g. Chapman *et al.*, 2015, Clarke *et al.*, 2013, El Korh *et al.*, 2009, Schröter *et al.*,
16
17 62 2004). In contrast, REE are mobilised and redistributed by processes involving melt (Plank &
18
19 63 Langmuir, 1993) and REE data is commonly used to determine evolving mineral assemblages
20
21 64 and P–T conditions in the arc root (e.g. Bignold *et al.*, 2006, Dalpé & Baker, 2000, Tulloch &
22
23 65 Kimbrough, 2003) and magma fractionation processes (e.g. Allibone *et al.*, 2009, Chapman *et*
24
25 66 *al.*, 2016, Cooper *et al.*, 2016, Davidson *et al.*, 2007, Smith, 2014, Stevenson *et al.*, 2005). In
26
27 67 principle, REE ratios and patterns in rocks and minerals may be informative of processes
28
29 68 involving melt. However, melt–rock interaction straddles the boundary between igneous and
30
31 69 metamorphic processes, involving melt but ultimately producing a metamorphic rock. The
32
33 70 presence of melt, as opposed to an aqueous fluid, is expected to increase chemical
34
35 71 communication and equilibration volumes. Therefore, melt presence may produce mineral
36
37 72 igneous chemical signatures in the modified rock, though the effects of protolith composition,
38
39 73 melt volume, and prevailing P–T conditions during melt–rock interaction have not been
40
41 74 extensively studied.

42
43
44
45
46
47
48 75 This contribution examines four styles of melt flux throughout a single, homogeneous
49
50 76 host rock, the Pembroke Granulite in Fiordland, Southern New Zealand. Previous work
51
52 77 examining melt flux has focused on field relationships and microstructures, demonstrating
53
54 78 that melt–rock interaction involved little to no crystallisation of melt within the modified
55
56 79 rocks, and the mineral assemblages and microstructures that were produced during melt–rock

1
2
3 80 interaction are common in lower crustal rocks (Daczko *et al.*, 2016, Stuart *et al.*, in press,
4
5 81 Stuart *et al.*, 2016). We analyse bulk rock composition and mineral major and trace element
6
7 82 compositions to investigate the link between chemical signatures, melt flux style and P–T
8
9 83 conditions of melt–rock interaction in the lower crust. Our findings indicate that the stable
10
11 84 assemblage and major element composition of minerals are defined by the P–T conditions at
12
13 85 the time of melt flux, like metamorphic assemblages. In contrast, mineral REE patterns are
14
15 86 characterised by signatures common in igneous rocks. We relate the strength of these igneous
16
17 87 signatures and relative homogeneity to the spatial extent and connectivity of the melt network
18
19 88 throughout the rock.
20
21
22

23 89 **GEOLOGICAL SETTING AND PREVIOUS WORK**

24 25 26 90 **Geological setting**

27
28
29 91 The Pembroke Granulite, Fiordland, New Zealand, is a low strain component of the Median
30
31 92 Batholith, a suite of Carboniferous to Early Cretaceous plutons emplaced into, and partly
32
33 93 comprising, the lower crust of a Cordilleran magmatic arc (Blattner, 1991, Mortimer *et al.*,
34
35 94 1999). Emplaced at 139–129 Ma (Hollis *et al.*, 2003), the gabbroic protolith to the Pembroke
36
37 95 Granulite had an igneous assemblage of enstatite, diopside, brown-green pargasite,
38
39 96 plagioclase, and ilmenite. The whole rock composition of the two-pyroxene–pargasite pluton
40
41 97 varies by several weight percent for all major element oxides (Stuart *et al.*, 2016). The
42
43 98 Pembroke Granulite, aside from some slight grain size variations, is otherwise homogeneous.
44
45 99 Igneous minerals were variably recrystallised during D₁ to form a gneissic foliation (S₁) that
46
47 100 strikes NE and dips steeply to the north and south. Similar assemblages in the nearby Western
48
49 101 Fiordland Orthogneiss formed at lower-crustal conditions of ~ 850°C and < 11 kbar (Daczko
50
51 102 & Halpin, 2009).
52
53
54
55
56
57
58
59
60

1
2
3 103 Emplacement and D₁ preceded a major pulse of high-Sr/Y magmatism in the arc
4
5 104 system (126–115 Ma; Allibone *et al.*, 2009, Hollis *et al.*, 2003, Hollis *et al.*, 2004, Milan *et*
6
7 105 *al.*, 2016, Tulloch & Kimbrough, 2003), and as such the Pembroke Granulite represents part
8
9 106 of the lower crust through which the high-Sr/Y melts migrated (Daczko *et al.*, 2016, Stuart *et*
10
11 107 *al.*, in press, Stuart *et al.*, 2016).

14 108 **Summary of styles of melt flux**

16
17 109 Melt–rock interaction, as the high-Sr/Y melts fluxed through the Pembroke Granulite,
18
19 110 resulted in four different styles of modification of the protolith two-pyroxene–pargasite
20
21 111 gneiss. Key changes common to all melt flux styles involve hydration and an increase in the
22
23 112 mode of amphibole (Fig. 1, Table 1). The first melt flux style involved widespread growth of
24
25 113 pargasite-bearing coronae around igneous and S₁ pyroxene throughout the entire Pembroke
26
27 114 Granulite (Style 1 [En + Di + Prg + Qtz + Pl + Czo + Rt ± Ap]; Stuart *et al.*, 2016). Each of
28
29 115 the later styles of melt–rock interaction (Styles 2–4) formed distinct minor rock types hosted
30
31 116 within the Pembroke Granulite, including tschermakite–clinozoisite gneiss and migmatite
32
33 117 (Style 2 [Ts + Grt + Czo + Pl + Ms + Qtz + Rt]; sometimes called dioritic gneiss in past
34
35 118 literature; Daczko *et al.*, 2001a, Daczko *et al.*, 2002a, Stuart *et al.*, in press), melt-bearing
36
37 119 high-grade shear zones (Style 3 [Ts + Grt + Czo + Pl + Ms + Qtz + Rt]; called D₃ and D₄
38
39 120 shear zones in past literature; Daczko *et al.*, 2001b, Gardner *et al.*, 2016), and hornblendite
40
41 121 (Style 4 [Prg ± Czo ± Pl ± Bt ± Grt ± Ru]; Daczko *et al.*, 2016, Meek, 2015). Previous work
42
43 122 suggests that each melt flux style is distinct in terms of volume of melt in the rock at any one
44
45 123 time, scale of melt-fluxed rock, the interpreted cumulate melt flux and whether flux was
46
47 124 deformation assisted or occurred under static conditions. The key characteristics of the four
48
49 125 styles of melt–rock interaction are summarised as follows. Mineral abbreviations used
50
51 126 throughout the manuscript follow the scheme proposed by Whitney and Evans (2010).
52
53
54
55
56
57
58
59
60

1
2
3 127 *Style 1: Diffuse porous melt flow*
4

5 128 The earliest style of melt–rock interaction occurred post-D₁ and involved flux of small
6
7 129 volumes of melt along grain boundaries throughout the bulk of the Pembroke Granulite
8
9 130 (Table 1; Fig. 1a; Stuart *et al.*, 2016). Initially, local small volumes (< 5%) of in situ partial
10
11 131 melting is inferred to have created a permeable grain boundary network, which was utilised as
12
13 132 pathways by an externally derived, high-Sr/Y melt. Melt–rock interaction involved partial
14
15 133 hydration and replacement of the two-pyroxene–pargasite gneiss (Fig. 1b), forming coronas
16
17 134 of blue-green pargasite and quartz (Fig. 1c) that are intimately associated with clinozoisite, Sr
18
19 135 enrichment in plagioclase and microstructures indicative of the former presence of melt (Fig.
20
21 136 1c, inset). Partial hydration of the S₁ assemblage is observed, to variable extent, throughout
22
23 137 the entirety of the Pembroke Granulite. Style 1 involves small volumes of melt fluxing
24
25 138 pervasively through the rock under static conditions, distributed on a large scale, with a
26
27 139 relatively small cumulate melt flux at an outcrop scale.
28
29
30
31
32

33 140 Partial hydration of S₁ in the two-pyroxene–pargasite gneiss by Style 1 melt flux is cut
34
35 141 by a series of sub-vertical anorthositic D₂ dykes, around which the assemblage is dehydrated
36
37 142 and transformed to garnet granulite at a scale of cm-dm, called garnet reaction zones (GRZ);
38
39 143 these are well-documented in the literature (Blattner, 1976, Clarke *et al.*, 2005, Clarke *et al.*,
40
41 144 2000, Daczko *et al.*, 2001a, Daczko & Halpin, 2009, Schröter *et al.*, 2004, Smith *et al.*, 2015).
42
43 145 All subsequent styles of melt flux (Styles 2, 3 and 4) overprint both the partially hydrated S₁
44
45 146 (Style 1) as well as GRZ.
46
47
48

49 147 *Style 2: Channelised porous melt flow*
50

51
52 148 Style 2 of melt flux is similar in nature to Style 1, except melt flux is concentrated into narrow
53
54 149 (<20 m wide) channels (Fig. 1d; Table 1; Stuart *et al.*, in press). Within the channels, melt–
55
56 150 rock interaction formed microstructures overprinting S₁, where zones of partial modification
57
58
59
60

1
2
3 151 form tschermakite-clinozoisite gneiss, and zones of complete modification form migmatite
4
5 152 (Fig. 1e). Modified rocks have hydrous assemblages dominated by tschermakite, clinozoisite
6
7 153 and plagioclase (Fig. 1f). Migmatites exhibit significant recrystallisation and contain coarse-
8
9 154 grained peritectic garnet interpreted as signatures of small volumes of in situ partial melting
10
11 155 (Fig. 1e and f). The degree of melt–rock interaction associated with Style 2 melt flux is more
12
13 156 extensive compared to Style 1, indicating either prolonged melt flux and/or higher cumulate
14
15 157 volumes of melt moving through the channels. Style 2 therefore involves intermediate
16
17 158 volumes of melt fluxing pervasively through the rock, concentrated within small channels and
18
19 159 under static conditions, with a relatively intermediate cumulate melt flux at an outcrop scale.
20
21
22

23
24 160 *Style 3: Deformation assisted porous melt flow*

25
26 161 Style 3 involves flux of melt along grain boundaries, where flux is spatially restricted within
27
28 162 D₃ shear zones (Fig. 1g; Table 1; these include the D₃ and D₄ shear zones of Daczko *et al.*
29
30 163 (2001b)). Two-pyroxene–pargasite gneiss, tschermakite–clinozoisite gneiss, and migmatite
31
32 164 are all deformed into shear zones (Fig. 1g and h) with assemblages dominated by
33
34 165 tschermakite, clinozoisite and plagioclase. Importantly, small amounts of syn-tectonic
35
36 166 medium-grained garnet (Fig. 1i) are observed (Daczko *et al.*, 2001b), interpreted as a
37
38 167 peritectic phase suggesting melt present conditions (Stuart *et al.*, in preparation). Ongoing
39
40 168 work reveals that microstructures indicative of the former presence of melt are ubiquitous
41
42 169 throughout shear zones (Fig. 1i, inset), consistent with published P–T conditions for
43
44 170 deformation which lie above the solidus (Table 1; Daczko *et al.*, 2001b). Studies show that
45
46 171 melt flux is more efficient in dynamic (deformation assisted) versus static conditions (e.g.
47
48 172 Daines & Kohlstedt, 1997, Davidson *et al.*, 1994, Rosenberg & Handy, 2000). Therefore,
49
50 173 volumes of melt moving through the shear zones are expected to be higher than those in
51
52 174 Styles 1 and 2. This is consistent with the complete hydration and overprinting of the S₁
53
54 175 assemblage within the shear zones (Fig. 1i). Style 3 is therefore interpreted to involve
55
56
57
58
59
60

1
2
3 176 intermediate volumes of melt fluxing pervasively through the deforming rock, concentrated
4
5 177 within zones of active shearing, with a relatively intermediate to high cumulate melt flux at
6
7 178 the outcrop scale.
8
9

10 179 *Style 4: Reactive infiltration followed by melt flux through an armoured zone*
11

12
13 180 Style 4 involves the deformation-assisted reactive infiltration of melt within a 30–40 m wide
14
15 181 channel forming a hornblendite (Fig. 1j; Table 1; Daczko *et al.*, 2016). Melt-rock interaction
16
17 182 results in dissolution of plagioclase and pyroxene, and the precipitation of pargasite with or
18
19 183 without clinozoisite (Fig. 1k). Local bands of garnet-rich rock are present (Daczko *et al.*,
20
21 184 2016). The complete dissolution of plagioclase–pyroxene and growth of pargasite ±
22
23 185 clinozoisite resulted in the formation of a channel that is unreactive with the fluxing melt.
24
25 186 Assisted by deformation, large volumes of melt may have fluxed efficiently through the
26
27 187 unreactive channel once it became armoured. Former melt is now pseudomorphed by minor
28
29 188 plagioclase (Fig. 1l, inset). The Style 4 hornblendite cuts rock types formed during Styles 1, 2
30
31 189 and 3. In summary, Style 4 is interpreted to involve large volumes of melt fluxing pervasively
32
33 190 through the deforming rock, concentrated within an armoured channel, with a relatively high
34
35 191 cumulate melt flux at an outcrop scale.
36
37
38
39

40 192 **SAMPLE SELECTION**

41
42
43 193 Data presented in this study are from representative rock types of all melt flux styles. Data for
44
45 194 Styles 1 and 2 stems from samples analysed in Stuart *et al.* (2016) and Stuart *et al.* (in press).
46
47 195 Raw data from these studies was collated with new data for Styles 3 and 4. Where possible,
48
49 196 samples were collected directly from outcrops, however in some cases rock types were
50
51 197 sampled from float in the creek after careful consideration of field relationships, characteristic
52
53 198 mineralogy and textures compared to the outcrops.
54
55

56 57 199 **METHODS**

1
2
3 200 **Whole rock composition**
4

5
6 201 Concentrations of major element oxides SiO₂, TiO₂, Al₂O₃, Fe₂O₃, MgO, MnO, CaO, Na₂O,
7
8 202 K₂O, P₂O₅ and SO₃ were determined for representative samples partially and completely
9
10 203 modified by Styles 3 and 4 using PANalytical PW2400 Sequential WDXRF Spectrometer
11
12 204 using WROXI standards (Mark Wainwright Analytical Centre at the University of New South
13
14 205 Wales, Sydney, Australia). Trace and rare earth elements were determined for select samples.
15
16 206 Digested samples were analysed on an Agilent 7500 series instrument using rock standards
17
18 207 BCR-2, BIR-1 and BHVO-2 for calibration (Geochemical Analysis Unit, CCFS/GEMOC,
19
20 208 Macquarie University, Sydney, Australia). Drift was corrected by spiking diluted samples
21
22 209 with Li, Ar, Rh and In.
23
24
25

26 210 **Mineral major element compositions**
27

28
29 211 Polished thin (30 µm) and thick (100 µm) sections were made from blocks cut from
30
31 212 representative samples; in the case of Style 3 samples blocks were cut perpendicular to
32
33 213 foliation and parallel to lineation. A petrographic microscope was used in combination with
34
35 214 the Virtual Petrographic Microscope (Tetley & Daczko, 2014), ImageJ 1.48a (Rasband,
36
37 215 1997–2015), and backscatter electron (BSE) images for mineral identification. BSE images
38
39 216 were collected using thin and thick sections coated with 10 nm of carbon in a Carl Zeiss IVO
40
41 217 scanning electron microscope (SEM; Geochemical Analysis Unit, Macquarie University,
42
43 218 Sydney, Australia). The SEM was run with an accelerating voltage of 15–20 kV, a beam
44
45 219 current of 10 nA and a working distance 10–12.5 mm.
46
47
48

49
50 220 Major element compositions of minerals were determined using a CAMECA SX100
51
52 221 electron microprobe (S₁, Styles 1, 2, and 4; Geochemical Analysis Unit, CCFS/GEMOC,
53
54 222 Macquarie University, Sydney, Australia) and a JEOL JXA8100 electron microprobe (Style
55
56 223 3; the Institute of Geology and Geophysics, Chinese Academy of Sciences (IGGCAS),
57
58
59
60

1
2
3 224 Beijing, China). Electron microprobes were run with accelerating voltages of 15 kV and beam
4
5 225 currents of 20 nA, analysing 1–5 μm spot sizes for 3.5–5 minutes per spot. Weight percent
6
7 226 oxide data were recalculated into cations per formula unit for individual minerals, using 23
8
9 227 oxygen for amphibole, 12 oxygen for garnet, 12.5 oxygen for clinozoisite and 8 oxygen for
10
11 228 feldspar. Amphibole classification and Fe^{3+} content calculation used the spreadsheet AMPH-
12
13 229 CLASS (Esawi, 2004). Fe^{3+} content in garnet was calculated by converting a portion of FeO
14
15 230 to Fe_2O_3 so the cations per formula unit sum to 8. Garnet end member proportions were then
16
17 231 calculated using the following: $\text{Alm} = 100 * \text{Fe}^{2+} / (\text{Fe}^{2+} + \text{Mg} + \text{Ca} + \text{Mn})$; $\text{Pyr} = 100 * \text{Mg} /$
18
19 232 $(\text{Fe}^{2+} + \text{Mg} + \text{Ca} + \text{Mn})$; $\text{Grs} = 100 * \text{Ca} / (\text{Fe}^{2+} + \text{Mg} + \text{Ca} + \text{Mn})$; and $\text{Sps} = 100 * \text{Mn} / (\text{Fe}^{2+}$
20
21 233 $+ \text{Mg} + \text{Ca} + \text{Mn})$. Plagioclase end member proportions were calculated using the following:
22
23 234 $\text{Ab} = 100 * \text{Na} / (\text{Na} + \text{Ca} + \text{K})$; $\text{An} = 100 * \text{Ca} / (\text{Na} + \text{Ca} + \text{K})$; and $\text{Or} = 100 * \text{K} / (\text{Na} + \text{Ca}$
24
25 235 $+ \text{K})$. Pistacite content in clinozoisite epidote was calculated using: $\text{Ps} = 100 * \text{Fe}^{3+} / (\text{Fe}^{3+} +$
26
27 236 $\text{Al}^{3+})$.

237 **Mineral trace element composition**

238 Trace element distribution mapping of representative, completely fluxed samples of Styles 1,
239 2, and 3 was performed on the X-Ray Fluorescence Microscopy beamline, using the Maia-
240 384 detector on the Kirkpatrick-Baez mirror microprobe at the Australian Synchrotron,
241 Melbourne (Paterson *et al.*, 2011, Ryan *et al.*, 2010b). Polished thin sections mounted on
242 glass slides were used for analysis; no additional preparation was performed. Maps were
243 made by scanning thin sections in 4 μm step sizes in the x and y directions at a speed of 4.096
244 mm/s and dwell time of 0.98 ms/pixel. Spot sizes of 4 μm^2 were analysed using a beam
245 energy of 18.5 keV. Standard foils (Pt, Mn, Fe, YF_3) were periodically analysed for
246 calibration. Real time processing, using the Dynamic Analysis (DA) method (Ryan, 2000,
247 Ryan *et al.*, 2010a), deconvolutes each individual X-ray event into element signals allowing
248 rapid data collection, high count rates and high sensitivity. Data reduction was performed

1
2
3 249 using GeoPIXE (Ryan *et al.*, 1990), which deconvolutes the spectra using the fundamental
4
5 250 parameter model for the layered sample, the Maia detector efficiency model, and the DA
6
7 251 matrix method. A pure plagioclase matrix, using concentrations of values from analysed
8
9 252 features in the samples and mineral densities, was used for matrix correction. Maps were
10
11 253 constructed for each sample to highlight relative zoning of Sr in plagioclase.
12
13

14 **Mineral rare earth element composition**

15
16
17 255 Rare earth element compositions of minerals were determined using laser ablation inductively
18
19 256 coupled plasma mass spectrometry (LA-ICP-MS). A Photon Machines Excite excimer 193
20
21 257 nm laser ablation microprobe system ablated 25–50 μm spots from thin sections at a
22
23 258 frequency of 5 Hz. Ablated material was transported in helium gas to the plasma at a flow rate
24
25 259 of 0.8 Lmin^{-1} . Material was analysed in an Agilent 7700x ICP-MS, using Ar as a carrier gas
26
27 260 with a flow rate of 1.0 Lmin^{-1} . Calcium (measured by EMP) was used as an internal standard
28
29 261 for all minerals, and NIST 610 glass, basalt from the Columbia River (BCR-2), and
30
31 262 MONGOL garnet were used as external standards. Raw signal data were reduced using the
32
33 263 GLITTER software (Griffin *et al.*, 2008). Rare earth element concentrations obtained from
34
35 264 GLITTER were normalised to chondrite values of McDonough and Sun (1995).
36
37
38
39

40 **P–T estimation**

41
42
43 266 Thermobarometry was used to obtain P–T conditions prevailing at the time of each melt flux
44
45 267 style. As amphibole is the only mineral common to all rock types, amphibole data were used
46
47 268 to obtain comparable results for each melt flux style. Compositions, including Fe^{3+} content,
48
49 269 were calculated to 13 cations per formula unit following the method of Leake *et al.* (1997),
50
51 270 and then used in the Ti-in-amphibole thermometer (Otten, 1984) and the Al-in-hornblende
52
53 271 barometer (Anderson & Smith, 1995, Hammarstrom & Zen, 1986, Hollister *et al.*, 1987). It
54
55 272 should be noted that results may not necessarily be true representations of the absolute P–T
56
57
58
59
60

1
2
3
4
5
6
7
8
9
10
11
12
13
14
15
16
17
18
19
20
21
22
23
24
25
26
27
28
29
30
31
32
33
34
35
36
37
38
39
40
41
42
43
44
45
46
47
48
49
50
51
52
53
54
55
56
57
58
59
60

273 conditions of melt flux, as the thermometer and barometer are intended for igneous
274 amphiboles; as such, we only use results to compare relative P–T changes between melt flux
275 styles.

276 **WHOLE ROCK COMPOSITION OF THE PEMBROKE GRANULITE**

277 Rocks fluxed by Styles 1, 2, and 3 are calc-alkaline, where most samples are monzodioritic or
278 monzogabbroic in composition (Fig. 2a), and some Style 3 samples fall within the gabbroic
279 field on the silica versus total alkali diagram of Middlemost (1994). Style 4 samples have
280 compositions distinct from the other styles, plotting in the foid-gabbroic field on the silica
281 versus total alkali diagram of Middlemost (1994), with lower SiO₂ (40.29–42.25 wt%; Fig.
282 2a). All samples are peraluminous, with Aluminium saturation of ~ 1.36 for Styles 1, 2, and 3,
283 and ~ 1.09 for Style 4, and Peacock indexes of ~ 0.24 for Styles 1, 2, and 3, and ~ 0.50 for
284 Style 4. All samples have low TiO₂ (0.42–1.99 wt%), high Al₂O₃ (16.74–20.44 wt%; Fig. 2b),
285 and high alkali content (Na₂O + K₂O = 2.55–6.18 wt%; Fig. 2a).

286 Samples exhibit small variation in all major element oxide concentrations, and overlap
287 within the compositional variation of Styles 1, 2, and 3 (Fig. 2b and c). Styles 1, 2, and 3, are
288 characterised by MgO of 3.88–6.34 wt% (Fig. 2c) and Sr/Y ratios of 36.5–221.1 (Fig. 2d). In
289 comparison, Style 4 samples have higher MgO (6.70–11.37 wt%; Fig. 2c) and lower Sr/Y
290 ratios (4.41–26.39; Fig. 2d). Style 4 samples also exhibit small variation in all major element
291 oxide concentrations. However, Style 4 samples bearing clinozoisite tend to have higher
292 Al₂O₃ and lower MgO than those without (Fig. 2b and c).

293 All styles have whole rock REE patterns enriched relative to chondrite. Styles 1 and 2
294 have negatively sloped REE patterns (LREE > 9 times chondrite, and MREE and HREE 1–11
295 times chondrite) and positive Eu anomalies (Fig. 2e). REE patterns of Style 4 clinozoisite
296 bearing samples have similarly shaped, negatively sloped REE patterns which are further

1
2
3 297 enriched compared to Styles 1 and 2 (LREE 20–90 times chondrite, MREE and HREE 2–25
4
5 298 times chondrite; Fig. 2f). Style 4 samples lacking clinozoisite have concave down patterns,
6
7 299 with inflections centred on Sm and larger variations in enrichment compared to chondrite
8
9 300 (Fig. 2f). Only one clinozoisite-bearing sample has a pronounced, positive Eu anomaly; other
10
11 301 samples show less pronounced, negative Eu anomalies or lack Eu anomalies.
12
13

14 302 **MINERAL COMPOSITIONS**

15 303 **Major elements**

16
17 304 Amphibole formed during S_1 and Styles 1 and 4 is pargasite (A site ($Na_A + K_A$) > 0.50, Fig.
18
19 305 3a), whereas amphibole formed during Styles 2 and 3 is tschermakite (A site < 0.50, Fig. 3a).
20
21 306 S_1 and Style 1 pargasite have overlapping compositions and exhibit the largest compositional
22
23 307 variation. Styles 2 and 3 tschermakite and Style 4 pargasite have smaller, more distinct ranges
24
25 308 in composition (Fig. 3a and b), where Style 2 tschermakite have low A site occupancy and
26
27 309 low Ti (~ 0.37 and ~ 0.06, respectively), Style 3 tschermakite have the lowest A site
28
29 310 occupancy and low Ti (~ 0.23 and ~ 0.05, respectively) and Style 4 pargasite have high A site
30
31 311 occupancy and high Ti (~ 0.61 and ~ 0.09, respectively). Within the distinct compositional
32
33 312 clusters for each Style, tschermakite in partially modified Style 2 samples have consistently
34
35 313 lower Ti compared to completely modified samples, whereas pargasite in Style 4 clinozoisite
36
37 314 bearing samples have consistently higher Ti compared to samples lacking clinozoisite (Fig.
38
39 315 3b).
40
41
42
43
44
45
46

47 316 Garnet formed during Style 2 is almandine with $Alm_{50-57}Pyr_{18-26}Grs_{16-23}Sps_{2-6}$ (Fig.
48
49 317 3c), with rims that are enriched in pyrope and depleted in grossular by 1–3% each. Garnet in
50
51 318 partially modified Style 2 samples is almandine–pyrope with $Alm_{36-45}Pyr_{32-42}Grs_{20-21}Sps_{1-3}$.
52
53 319 Garnet formed during Style 3 is almandine with $Alm_{51-60}Pyr_{15-30}Grs_{14-21}Sps_{1-10}$, with minor
54
55 320 zoning of Ca rich rims observed. Garnet formed during Style 4 is almandine–grossular with
56
57
58
59
60

1
2
3 321 Alm_{44–53}Pyr_{17–25}Gr_{25–32}Sps_{2–4}, and lacks chemical zoning. Fe³⁺ content in Style 2 garnet is
4
5 322 0.06–0.20 cpfu, whereas Style 3 and 4 garnets are within error of no Fe³⁺ content.
6
7

8 323 Clinozoisite shows minor variations in Fe³⁺ substitution by Al³⁺, with little appreciable
9
10 324 compositional difference between those formed in the different melt flux styles. Pistacite
11
12 325 content ranges between 12 and 18 (Fig. 3d), where Style 1 clinozoisite have higher values
13
14 326 (16–18), and Styles 2, 3, and 4 have wider ranges in composition.
15
16

17 327 Plagioclase deformed in S₁ has X_{Ab} = 58–66 (Fig. S1), and classify as andesine. In
18
19 328 contrast, plagioclase formed in the different melt flux styles is typically more albitic; Styles 1,
20
21 329 2, and 3 plagioclase analyses classify as andesine or oligoclase (X_{Ab} = 53–80, 66–76, and 67–
22
23 330 75 respectively), and Style 4 plagioclase has high X_{Ab} (77–87) and is either oligoclase or
24
25 331 albite. Within Style 2, partially modified samples have a wider compositional range (X_{Ab} =
26
27 332 53–76) compared to completely modified samples (X_{Ab} = 73–76). Minor K-feldspar occurring
28
29 333 in melt pseudomorphs in Style 4 hornblendites are orthoclase (X_{Or} = 98).
30
31
32

33 334 **Sr trace element mapping**

34
35
36 335 Synchrotron element mapping shows significant zoning of Sr both at the map scale and within
37
38 336 individual grains of plagioclase associated with the different melt flux styles. Within a Style 1
39
40 337 sample, plagioclase (approx. 70 vol%) can be divided into 1–2 mm wide bands of high- and
41
42 338 low-Sr traversing the thin section (Fig. 4a). High-Sr bands closely follow pyroxene–
43
44 339 plagioclase boundaries and are spatially associated with replacement microstructures of
45
46 340 pargasite and quartz, Style 1 melt–rock interaction products. Coarse-grained plagioclase (0.9–
47
48 341 2.0 mm) are zoned in Sr, where high-Sr grain boundaries are adjacent to replacement
49
50 342 microstructures forming the high-Sr bands, and low-Sr grain boundaries are next to other
51
52 343 plagioclase grains which are also low in Sr.
53
54
55
56
57
58
59
60

1
2
3 344 Similar map-scale and grain-scale zoning are observed in a Style 2 sample (Fig. 4b).
4
5 345 Sr zoning in plagioclase (approx. 40 vol%) is present throughout the map and is not spatially
6
7 346 associated with microstructures or minerals. The map can be divided into bands of higher and
8
9 347 lower Sr enrichment, up to 5 mm wide that are oriented vertically across the map and are sub-
10
11 348 parallel with a composite S_1 / S_3 . The high-Sr band comprises many plagioclase grains (100–
12
13 349 800 μm) that are enriched in Sr. Similarly, low-Sr bands comprise many grains that have
14
15 350 relatively low Sr. Individual grains in both the high- and low-Sr bands are themselves
16
17 351 asymmetrically zoned in Sr, where grains have high- and low-Sr grain boundaries that bear no
18
19 352 relation to grain boundaries of adjacent grains (i.e. a high-Sr boundary of one grain may be
20
21 353 adjacent to a low-Sr boundary of a neighbouring grain).
22
23
24

25
26 354 Style 3 samples have less pronounced map-scale and grain-scale zoning compared to
27
28 355 Styles 1 and 2 (Fig. 4c). Map-scale zoning involves only slight relative changes to the overall
29
30 356 Sr content in plagioclase (approx. 40 vol%). One high-Sr band, approximately 5 mm wide, is
31
32 357 associated with the coarse-grained garnet on the far right of the map. Many individual grains
33
34 358 exhibit homogeneous Sr content; however, some rare grains have minor asymmetric Sr
35
36 359 zoning.
37
38

39 360 **Rare earth element mineral compositions**

40
41
42 361 Amphiboles from S_1 and Style 1 have enriched patterns with gentle convex shapes from La to
43
44 362 Sm (1–27 times chondrite; Fig. 5), small, positive Eu anomalies and flat MREE and HREE
45
46 363 (4–19 times chondrite). In comparison, Style 2 amphiboles become progressively depleted in
47
48 364 REE, with less pronounced Eu anomalies. Partially modified Style 2 samples have a wide
49
50 365 range of depleted LREE values (0.01–1 times chondrite) which increase towards flat, enriched
51
52 366 MREE to HREE (1–9 times chondrite). Completely modified Style 2 samples have LREE
53
54 367 values below detection limits, and increasing patterns from MREE to HREE (0.4–5 times
55
56
57
58
59
60

1
2
3 368 chondrite). Partially and completely modified Style 3 amphiboles have similar patterns, with
4
5 369 wide ranges in LREE from enriched, flat patterns (1–5 times chondrite) to depleted, sloped
6
7 370 patterns (0.01–1 times chondrite). MREE and HREE are flat, approximately 1 times chondrite
8
9 371 in partially modified samples and slightly more enriched in completely modified samples (1–4
10
11 372 times chondrite). All patterns have weak, positive Eu anomalies. Style 4 amphiboles have
12
13 373 increasing trends from La to Eu (0.04–2.6 times chondrite) to flat, enriched MREE and HREE
14
15 374 (up to 6 times chondrite).
16
17
18

19 375 Garnets from Style 2 samples have LREE below detection limits, and MREE define an
20
21 376 increasing trend to HREE (1–56 times chondrite; Fig. 5). Style 3 garnets have three different
22
23 377 REE patterns. One is defined by increasing REE patterns from depleted LREE to enriched
24
25 378 MREE, with an inflection point at Sm (~25 times chondrite), a weak positive or neutral Eu
26
27 379 anomaly and flat, enriched HREE patterns (~30 times chondrite). A second pattern is
28
29 380 comparatively depleted in HREE compared to the first (1–10 times chondrite), with
30
31 381 decreasing patterns from Dy to Ho. A third pattern is comparatively depleted in LREE and
32
33 382 MREE (below detection limits and 0.6–5 times chondrite, respectively), and has increasing
34
35 383 trends from Dy to Lu (up to ~40 times chondrite). In clinozoisite-bearing Style 4 samples,
36
37 384 garnets have two patterns. One pattern is defined by an overall increasing trend from depleted
38
39 385 LREE (below detection limits to 6 times chondrite) to enriched HREE (up to 23 times
40
41 386 chondrite), with a decrease between Eu and Gd defining a strong, positive Eu anomaly. The
42
43 387 second pattern also has an increasing trend from depleted LREE to enriched HREE, however
44
45 388 has either a neutral or weak positive Eu anomaly, depleted LREE and a slight inflection
46
47 389 between La and Ce forming an inverted spoon shaped pattern. This second, inverted spoon
48
49 390 shaped pattern is typical of garnets in Style 4 samples lacking clinozoisite, which may be
50
51 391 further enriched up to 250 times chondrite. Eu anomalies may be either weakly positive,
52
53 392 weakly negative or neutral.
54
55
56
57
58
59
60

1
2
3 393 In all samples, clinozoisite has enriched REE patterns (1–1300 times chondrite; Fig. 5)
4
5 394 defined by decreasing trends from La to Lu, with positive Eu anomalies of varying
6
7 395 magnitude. Partially modified Style 2 clinozoisite grains have strong Eu anomalies, and
8
9 396 HREE tend to be flat rather than sloped. Completely modified Style 2 clinozoisite are more
10
11 397 enriched than partially modified clinozoisite, and have steeper HREE patterns. Style 3
12
13 398 clinozoisite have a mix of flat and steep HREE trends in both partially and completely
14
15 399 modified samples, and range between 1 and 225 times chondrite. Style 4 clinozoisite also
16
17 400 show flat and steep HREE trends, where flat HREE profiles come from cores of grains and
18
19 401 steep profiles from rims.

22 402 **P–T CONSTRAINTS**

23
24
25
26 403 P–T conditions for both S₁ and Style 1 form a trend from low-P, high-T to high-P, low-T over
27
28 404 a range of ~300°C and ~11 kbar (Fig. 6). Lying along this trend at the high-P, low-T end,
29
30 405 Styles 2, 3, and 4 have smaller ranges in calculated P–T space. Style 2 has partially modified
31
32 406 samples at temperatures ~30°C lower than the completely modified samples, which cluster
33
34 407 around 600°C and 10.5–11 kbar. Style 3 samples have similar temperatures compared to Style
35
36 408 2, and pressures of ~11 kbar. No difference between partially and completely modified
37
38 409 samples of Style 3 is observed. Style 4 samples lie at temperatures ~30°C higher than Styles 2
39
40 410 and 3, and have larger variation in pressure (9–13 kbar). Style 4 samples bearing clinozoisite
41
42 411 typically have temperatures ~20°C higher than those without clinozoisite.

46 412 **DISCUSSION**

49 413 **Different melt flux styles – different P–T conditions?**

50
51
52 414 Garnet-bearing assemblages in mafic to intermediate metaigneous rocks are indicative of
53
54 415 high-P metamorphism and, in some cases, partial melting (De Paoli *et al.*, 2012, O'Brien &
55
56 416 Rötzler, 2003, Pattison, 2003). Previous studies have shown that large volumes of the

1
2
3 417 Fiordland lower crust, including the Pembroke Granulite, experienced burial and
4
5 418 recrystallisation at high-P during a period of voluminous high-Sr/Y pluton emplacement at
6
7 419 125–114 Ma (Bradshaw, 1989, Chapman *et al.*, 2015, Clarke *et al.*, 2000, Daczko *et al.*,
8
9 420 2002a, Daczko & Halpin, 2009, Daczko *et al.*, 2009, Daczko *et al.*, 2002b, De Paoli *et al.*,
10
11 421 2009, Hollis *et al.*, 2003, Hollis *et al.*, 2004, Milan *et al.*, 2016, Stowell *et al.*, 2014, Stowell
12
13 422 *et al.*, 2010). The four styles of melt flux observed in the Pembroke Granulite are interpreted
14
15 423 as records of migration of these high-Sr/Y magmas (Stuart *et al.*, 2016), albeit with different
16
17 424 chemical signatures and at different P–T conditions. Our P–T calculations are less than
18
19 425 published values for the Pembroke Granulite (Clarke *et al.*, 2000, Daczko *et al.*, 2001a,
20
21 426 Daczko *et al.*, 2001b, Stowell *et al.*, 2010, Stuart *et al.*, 2016) because they are based solely
22
23 427 on amphibole composition. Therefore, we only take the relative P–T conditions of the
24
25 428 different styles, as opposed to the absolute estimate of pressure or temperature, into
26
27 429 consideration here.

31
32 430 P–T estimates for Style 1 melt flux (Fig. 6; Stuart *et al.*, 2016) suggest that the garnet
33
34 431 absent, pargasite-quartz symplectites around pyroxene grains (Fig. 1c) formed at pressures
35
36 432 <12 kbar. Variability in amphibole compositions (Fig. 4a) and a lack of widespread
37
38 433 recrystallisation (Stuart *et al.*, 2016) likely reflects a lack of outcrop-scale equilibrium during
39
40 434 melt-flux. Consequently, calculated pressures and temperatures (Fig. 6) may represent a mix
41
42 435 between S₁ P–T conditions and Style 1 P–T conditions. The preservation of the mineral
43
44 436 chemical signature of Style 1 melt flux suggests that the mineral assemblage did not re-
45
46 437 equilibrate at high pressure conditions during subsequent channelled melt–rock interaction.
47
48 438 Tschermakite, garnet and plagioclase bearing assemblages that completely replace the Style 1
49
50 439 assemblage in channels of Styles 2 and 3 melt flux have small ranges in mineral compositions
51
52 440 and small ranges in calculated P–T conditions at high pressures and comparatively lower
53
54 441 temperatures. Our P–T estimates are <60°C and <3 kbar below published values for Style 2
55
56
57
58
59
60

1
2
3 442 (partial melting; Daczko *et al.*, 2001a, Daczko & Halpin, 2009) and Style 3 (shearing; Daczko
4
5 443 *et al.*, 2001b). However, the relative temperature calculations for Style 2 fit with a lower
6
7 444 temperature for partially modified samples compared with completely modified samples of
8
9 445 Styles 2 and 3 that display minor amounts (<5 vol%) of in situ partial melting, indicating the
10
11 446 solidus lies at the high-T side of partially modified Style 2 samples (Fig. 6, inset).

12
13
14 447 Plagioclase-absent assemblages from Style 4 formed at temperatures ~ 30°C higher
15
16 448 than plagioclase-bearing assemblages from Styles 2 and 3 (Fig. 6). Crystallisation
17
18 449 experiments in mafic to intermediate magmas show that plagioclase is stable at lower
19
20 450 temperatures and pressures close to the solidus, and that the plagioclase-out line is at higher
21
22 451 temperature for intermediate compared to mafic compositions (Green, 1982). Therefore,
23
24 452 subtly higher temperatures (Fig. 6, inset) and/or a more mafic melt accompanied Style 4 melt
25
26 453 flux and dramatically changed the character of melt–rock interaction by destabilising
27
28 454 plagioclase in the presence of the externally-derived melt. This switch may have been caused
29
30 455 by advection of heat during extended or more voluminous fluxing of the externally derived
31
32 456 melt and/or a shift to a more mafic character of the fluxing melt as the channel became
33
34 457 armoured and less reactive. A localised temperature increase is supported by evidence for
35
36 458 partial melting in a metre-scale transition zone that separates the Style 4 hornblende body
37
38 459 from the unmelted, precursor two-pyroxene–pargasite gneiss (Daczko *et al.*, 2016). As such,
39
40 460 Style 4 also describes a history of melt flux at conditions above the solidus within the
41
42 461 Fiordland lower crust.

43 462 **Homogeneous versus heterogeneous whole rock compositions**

44
45
46 463 Preservation of S₁ assemblages and partial modification during each style of melt–rock
47
48 464 interaction provides the opportunity to evaluate the chemical evolution of both the bulk rock
49
50 465 and the mineralogy during different styles of melt–rock interaction. Each style of melt–rock
51
52
53
54
55
56
57
58
59
60

1
2
3 466 interaction is subtly different, however the presence of a grain boundary network of melt, a
4
5 467 bulk hydration effect and the growth of amphibole are common to all four styles.
6
7

8 468 During flux, melt is interpreted to pass through the Pembroke Granulite with only
9
10 469 small volumes of melt crystallising in place, implying that any variation in bulk composition
11
12 470 is a result of melt-driven metasomatism. Rock types formed by melt–rock interaction during
13
14 471 Styles 1, 2, and 3 have bulk rock compositions indistinct from the precursor two-pyroxene–
15
16 472 pargasite gneiss (Fig. 2; excluding volatile content). This includes a few samples of Style 3
17
18 473 that plot in the gabbroic field of Fig. 2a and are interpreted as sampling of slightly more mafic
19
20 474 primary components of the Pembroke Granulite. Homogeneous bulk compositions in Styles 1,
21
22 475 2, and 3 overlapping with the precursor two-pyroxene–pargasite gneiss are consistent with
23
24 476 nearly isochemical melt–rock interaction. In contrast, major and REE element compositions
25
26 477 of Style 4 samples are different to that of the precursor rock (Fig. 2), consistent with melt–
27
28 478 driven metasomatism during flux. In the case of Style 4, the melt–rock interaction occurred at
29
30 479 higher temperatures, facilitating significant reaction and mass exchange during flux.
31
32
33
34

35 480 **Major element mineral chemistry and partitioning of rare earth elements in the**
36
37 481 **presence of melt**
38
39

40 482 Despite melt-driven metasomatism during melt–rock interaction, compositions of minerals
41
42 483 from Style 4 are similar to, or overlap, compositions of minerals from the precursor rock and
43
44 484 Styles 1, 2, and 3 (Fig. 3). Variations in mineral compositions between Styles 1, 2, and 3 are
45
46 485 difficult to link to melt-driven metasomatism when bulk rock compositions are homogeneous.
47
48 486 However, each melt flux style occurred at subtly different P–T–X conditions, and
49
50 487 equilibration at these varying conditions may have imparted distinct mineral assemblages and
51
52 488 compositions for each style. The composition of Style 1 amphiboles (Fig. 3a and b) and
53
54 489 distribution of Sr in Style 1 plagioclase (Fig. 4a) varies considerably. A corresponding range
55
56
57
58
59
60

1
2
3 490 in calculated P–T conditions (Fig. 6) speaks to a lack of widespread equilibration during melt-
4
5 491 rock interaction. Small ranges in mineral compositions in Styles 2, 3, and 4 (Fig. 3), and less
6
7 492 pronounced Sr zoning in plagioclase (Fig. 4b and c) are indicative of widespread modification
8
9 493 and better equilibration during melt-rock interaction. Homogeneity in major element mineral
10
11 494 composition is most likely related to the cumulate volume of melt flux and the resulting
12
13 495 degree of modification and recrystallisation. Style 1 involves a small cumulate volume of melt
14
15 496 during flux and as such the S₁ assemblage is only partially modified; in comparison, the later
16
17 497 styles of melt flux involve larger cumulate volumes of melt and a more extensive
18
19 498 modification and recrystallisation of the host rock.
20
21
22

23 499 Rare earth element (REE) mineral chemistry (Fig. 5) suggests there was significant
24
25 500 redistribution of REE between minerals during melt-rock interaction, but little enrichment or
26
27 501 depletion occurred at a bulk rock scale except for Style 4 (Fig. 2f). In most cases, minerals
28
29 502 have homogeneous REE patterns, despite forming in reactions where they replace precursor
30
31 503 minerals with heterogeneous REE contents (e.g. Stuart *et al.*, 2016). Homogenisation of REE
32
33 504 patterns in metamorphic products is facilitated by the presence of an intergranular network of
34
35 505 melt, providing fast diffusion pathways (Acosta-Vigil *et al.*, 2012, Leshner, 1994, Mann, 1980)
36
37 506 at an outcrop scale. Compared to Styles 1, 2, and 4, amphibole and garnet formed in Style 3
38
39 507 melt flux have significant heterogeneities in their REE patterns, particularly in the LREE (Fig.
40
41 508 5). Given that LREE are strongly partitioned into clinozoisite (Beard *et al.*, 2006, Frei *et al.*,
42
43 509 2004, Frei *et al.*, 2003, Mulrooney & Rivers, 2005), heterogeneous LREE patterns are likely a
44
45 510 result of equilibration with varying proportions of clinozoisite. Style 3 is distinguished from
46
47 511 the other styles by significant deformation during melt flux, which may localise melt flux
48
49 512 (Baltzell *et al.*, 2015, Bauer *et al.*, 2000, Holtzman *et al.*, 2003, Rosenberg & Handy, 2000),
50
51 513 limiting connectivity and effectively reducing the volume of rock in chemical communication.
52
53 514 Therefore, the spatial extent or connectivity of the melt network may dictate the equilibration
54
55
56
57
58
59
60

1
2
3 515 volume and resulting homogeneity of REE compositions for each mineral. In this dynamic
4
5 516 case, Style 3 may also have experienced multiple episodes of structural reactivation and
6
7 517 repeated periods of melt flux, possibly by melts of variable composition. This may also
8
9 518 contribute to the heterogeneous nature of mineral REE compositions.

10
11
12 519 The broadly homogeneous REE patterns in melt–rock interaction products such as
13
14 520 garnet, amphibole, and clinozoisite highlight the extent to which the REE are partitioned
15
16 521 between the solid minerals and melt, in this P–T space straddling the boundary between
17
18 522 igneous and sub-solidus metamorphic processes. We have evaluated published REE patterns
19
20 523 of amphibole and clinozoisite formed under igneous versus sub-solidus metamorphic
21
22 524 conditions (Dalpé & Baker, 2000, El Korh *et al.*, 2009, Gromet & Silver, 1983) and compared
23
24 525 them to those obtained in this contribution involving melt–rock interaction. Published values
25
26 526 for sub-solidus metamorphic clinozoisite/epidote (Fig. 7a) are all enriched relative to
27
28 527 chondrite with overlapping, flat REE patterns. The pattern for igneous clinozoisite/epidote is
29
30 528 different to the metamorphic patterns, with enriched LREE relative to HREE forming a sloped
31
32 529 pattern. This closely matches average REE patterns of clinozoisite grains formed during melt-
33
34 530 rock interaction in the Pembroke Granulite (Fig. 7b). Published amphibole REE patterns can
35
36 531 be clearly divided into igneous, which are enriched with humps from La to Dy and flat HREE,
37
38 532 versus sub-solidus metamorphic, which are flat and depleted relative to chondrite (Fig. 7c).
39
40 533 Amphiboles formed during melt-rock interaction in the Pembroke Granulite are slightly more
41
42 534 ambiguous, with characteristics of both types of published patterns. In general, the amphibole
43
44 535 grains formed during Styles 1–4 melt flux have igneous-like, flat, enriched patterns from Gd
45
46 536 to Lu (Fig. 7d). S₁ and Style 1 amphiboles have a LREE hump, like igneous patterns from the
47
48 537 literature. It is important to note that Style 1 amphiboles are forming in an assemblage where
49
50 538 only minor amounts of clinozoisite are stable, and garnet is not stable. Thus, amphiboles are
51
52 539 not in competition for the REE available. Amphibole in Styles 2, 3, and 4 have depleted,
53
54
55
56
57
58
59
60

1
2
3 540 sloped LREE. Depletion is more characteristic of a metamorphic signature, and as discussed
4
5 541 above may be a result of partitioning with varying amounts of clinozoisite. However, unlike
6
7 542 the metamorphic patterns the LREE have a slope from La to Eu, which is closer to the shape
8
9 543 of igneous-like patterns. Overall, amphibole and clinozoisite REE patterns share more
10
11 544 similarities with published igneous REE patterns. Recrystallisation in the presence of melt,
12
13 545 and the large equilibration volume provided by the melt network are two factors which have
14
15 546 likely contributed to the formation of these igneous-like REE signatures.

19 547 **Generating igneous-like mineral chemical signatures in a metamorphic rock**

20
21
22 548 Differences in inferred melt flux between each style highlight a role for physical processes in
23
24 549 the formation of an igneous-like mineral chemical signature during melt–rock interaction. P–
25
26 550 T–X conditions of melt flux control both the stable assemblage and the major element
27
28 551 composition of the minerals. In the case of the Pembroke Granulite, the assemblage of
29
30 552 modified rock types is related to temperature and/or melt composition, demonstrated in the
31
32 553 instability of plagioclase during Style 4 melt flux. Major element compositions of minerals
33
34 554 formed during melt–rock interaction are determined by the P–T–X conditions of melt flux, as
35
36 555 in sub-solidus metamorphic systems. The homogeneity of mineral major element
37
38 556 compositions, or degree of equilibrium, is here inferred to relate to the cumulate volume of
39
40 557 melt flux, where smaller cumulate melt fluxes inhibit extensive equilibration, resulting in
41
42 558 heterogeneous mineral major element compositions as in Style 1. On the other hand, REE
43
44 559 compositions of minerals are more homogeneous and have igneous-like signatures, where
45
46 560 networks of melt provide large equilibration volumes for each mineral. In this case, the
47
48 561 strength of the igneous-like signature and degree of homogeneity relies on the spatial
49
50 562 distribution and connectivity of the melt network, which may be limited by deformation, such
51
52 563 as in Style 3.
53
54
55
56
57
58
59
60

1
2
3 564 Episodes of melt flux through the Pembroke Granulite are interpreted in the literature
4
5 565 based on field relationships and microstructural indicators. Excellent exposure of a relatively
6
7 566 homogeneous rock type with a spectacular grid of garnet reaction zones that form exceptional
8
9 567 markers for subsequent deformation and reaction permitted identification of melt–rock
10
11 568 interaction in the Pembroke Granulite (Daczko *et al.*, 2016, Stuart *et al.*, in press). These
12
13 569 workers examined continuous progressions from the precursor two-pyroxene–pargasite gneiss
14
15 570 to rock types modified by melt–rock interaction. In the absence of these extraordinary field
16
17 571 relationships and exposures, the amphibole-bearing rock types may be mistakenly identified
18
19 572 as primary igneous rocks, including cumulates. Microstructural indicators of the former
20
21 573 presence of melt in these rocks include: dihedral angles of $< 60^\circ$ at triple point junctions; three
22
23 574 mineral, granitic (plagioclase, quartz, K-feldspar) aggregates; pseudomorphing of
24
25 575 phyllosilicate minerals by plagioclase; cusped volumes of plagioclase and/or quartz; and
26
27 576 films of plagioclase and/or quartz along grain boundaries (Daczko *et al.*, 2016, Stuart *et al.*, in
28
29 577 press, Stuart *et al.*, 2016). Microstructural indicators of melt–rock interaction may now be
30
31 578 supported by the observation of an igneous-like REE mineral chemical signature within a
32
33 579 metamorphic rock. Together, the microstructural and mineral chemical signatures are a
34
35 580 powerful indicator of melt–rock interaction.
36
37
38
39
40

41 **CONCLUSIONS**

42
43
44 582 Melt–rock interaction during melt flux through the root of a magmatic arc has produced new
45
46 583 assemblages and broadly homogeneous mineral compositions at an outcrop scale. The P–T–X
47
48 584 conditions of melt flux generates new mineral assemblages and controls major element
49
50 585 compositions, as in sub-solidus metamorphic systems. Igneous-like REE patterns in minerals
51
52 586 formed in the presence of a grain boundary network of melt, and are identified as geochemical
53
54 587 signatures recording the former flux of melt. The network of melt enhanced equilibration
55
56 588 volumes and the mobility of REE at an outcrop scale. The cumulate flux of melt and spatial
57
58
59
60

1
2
3 589 distribution of melt network influence the degree of homogeneity and strength of the igneous-
4
5 590 like mineral REE signature. Comparison of the four different melt flux styles examined in this
6
7 591 study highlights the role that the physical characteristics of melt flux plays in generating the
8
9 592 geochemical signatures.

10 11 12 593 **ACKNOWLEDGEMENTS**

13
14
15 594 ARC Future Fellowship (FT110100070) to S.P., a Discovery Project funding (DP120102060)
16
17 595 to S.P. and NRD, and Australian Government Research Training Program Scholarships to
18
19 596 C.A.S. and U.M. provided financial support to conduct this research. We thank the
20
21 597 Department of Conservation, New Zealand for permission to visit and sample localities in the
22
23 598 Fiordland National Park. Part of this research was undertaken on the X-Ray Fluorescence
24
25 599 Microscopy beamline at the Australian Synchrotron, Victoria, Australia. This work was
26
27 600 supported by the Multi-modal Australian ScienceS Imaging and Visualisation Environment
28
29 601 (MASSIVE) (www.massive.org.au). This study used instrumentation funded by ARC LIEF
30
31 602 and DEST Systemic Infrastructure Grants, Macquarie University and Industry. This is
32
33 603 contribution XXX from the ARC Centre of Excellence for Core to Crust Fluid Systems
34
35 604 (www.ccfs.mq.edu.au) and XXXX from the GEMOC Key Centre (www.gemoc.mq.edu.au).

36 37 38 39 605 **SUPPLEMENTARY DATA**

40
41
42 606 Supplementary data for this paper, including Fig. S1 (Plagioclase albite composition), whole
43
44 607 rock composition, and mineral major and REE compositions are available at *Journal of*
45
46 608 *Petrology* online.

47 48 49 609 **REFERENCES**

50
51
52 610 Acosta-Vigil, A., London, D. & Morgan VI, G. B. (2012). Chemical diffusion of major
53
54 611 components in granitic liquids: Implications for the rates of homogenization of crustal melts.
55
56 612 *Lithos* **153**, 308–323.

- 1
2
3 613 Allibone, A. H., Jongens, R., Turnbull, I. M., Milan, L. A., Daczko, N. R., DePaoli, M. C. &
4
5 614 Tulloch, A. J. (2009). Plutonic rocks of Western Fiordland, New Zealand: Field relations,
6
7 615 geochemistry, correlation, and nomenclature. *New Zealand Journal of Geology and*
8
9 616 *Geophysics* **52**, 379–415.
- 11 617 Anderson, J. L. & Smith, D. R. (1995). The effects of temperature and f_{O_2} on the Al-in-
13
14 618 hornblende barometer. *American Mineralogist* **80**, 549–559.
- 16 619 Baltzell, C., Parmentier, E. M., Liang, Y. & Tirupathi, S. (2015). A high-order numerical
17
18 620 study of reactive dissolution in an upwelling heterogeneous mantle: 2. Effect of shear
19
20 621 deformation. *Geochemistry, Geophysics, Geosystems* **16**, 3855–3869.
- 22 622 Bauer, P., Palm, S. & Handy, M. R. (2000). Strain localization and fluid pathways in
23
24 623 mylonite: inferences from in situ deformation of a water-bearing quartz analogue
25
26 624 (norcamphor). *Tectonophysics* **320**, 141–165.
- 28 625 Beard, J. S., Sorensen, S. S. & Gieré, R. (2006). REE zoning in allanite related to changing
29
30 626 partition coefficients during crystallization: implications for REE behaviour in an epidote-
31
32 627 bearing tonalite. *Mineralogical Magazine* **70**, 419–436.
- 34 628 Bignold, S. M., Treloar, P. J. & Petford, N. (2006). Changing sources of magma generation
35
36 629 beneath intra-oceanic island arcs: An insight from the juvenile Kohistan island arc, Pakistan
37
38 630 Himalaya. *Chemical Geology* **233**, 46–74.
- 40 631 Blattner, P. (1976). Replacement of hornblende by garnet in granulite facies assemblages near
41
42 632 Milford Sound, New Zealand. *Contributions to Mineralogy and Petrology* **55**, 181–190.
- 44 633 Blattner, P. (1991). The north Fiordland transcurrent convergence. *New Zealand Journal of*
45
46 634 *Geology and Geophysics* **34**, 533–542.
- 48 635 Bradshaw, J. (1989). Early Cretaceous vein-related garnet granulite in Fiordland, southwest
49
50 636 New Zealand: A case for infiltration of mantle-derived-rich fluids. *The Journal of geology*,
51
52 637 697–717.

- 1
2
3 638 Chapman, T., Clarke, G. L. & Daczko, N. R. (2016). Crustal differentiation in a thickened arc
4
5 639 - evaluating depth dependences. *Journal of Petrology* **57**, 595–620.
6
7 640 Chapman, T., Clarke, G. L., Daczko, N. R., Piaolo, S. & Rajkumar, A. (2015).
8
9 641 Orthopyroxene–omphacite- and garnet–omphacite-bearing magmatic assemblages, Breaksea
10
11 642 Orthogneiss, New Zealand: Oxidation state controlled by high-P oxide fractionation. *Lithos*
12
13 643 **216–217**, 1–16.
14
15 644 Cherniak, D. J. (2003). REE diffusion in feldspar. *Chemical Geology* **193**, 25–41.
16
17 645 Chernoff, C. B. & Carlson, W. D. (1999). Trace element zoning as a record of chemical
18
19 646 disequilibrium during garnet growth. *Geology* **27**, 555–558.
20
21 647 Clarke, G., Daczko, N. R. & Miescher, D. (2013). Identifying relic igneous garnet and
22
23 648 clinopyroxene in eclogite and granulite, Breaksea Orthogneiss, New Zealand. *Journal of*
24
25 649 *Petrology* **54**, 1921–1938.
26
27 650 Clarke, G. L., Daczko, N. R., Klepeis, K. A. & Rushmer, T. (2005). Roles for fluid and/or
28
29 651 melt advection in forming high-*P* mafic migmatites, Fiordland, New Zealand. *Journal of*
30
31 652 *Metamorphic Geology* **23**, 557–567.
32
33 653 Clarke, G. L., Klepeis, K. A. & Daczko, N. R. (2000). Cretaceous high-*P* granulites at
34
35 654 Milford Sound, New Zealand: metamorphic history and emplacement in a convergent margin
36
37 655 setting. *Journal of Metamorphic Geology* **18**, 359–374.
38
39 656 Cooper, G. F., Davidson, J. P. & Blundy, J. D. (2016). Plutonic xenoliths from Martinique,
40
41 657 Lesser Antilles: evidence for open system processes and reactive melt flow in island arc crust.
42
43 658 *Contributions to Mineralogy and Petrology* **171**, 87.
44
45 659 Cullers, R. L. & Graf, J. L. (1984). Rare earth elements in igneous rocks of the continental
46
47 660 crust: Intermediate and silicic rocks–ore petrogenesis. In: Henderson, P. (ed.) *Rare Earth*
48
49 661 *Element Geochemistry*. Amsterdam: Elsevier, 275–308.
50
51
52
53
54
55
56
57
58
59
60

- 1
2
3 662 Cullers, R. L., Medaris, L. G. & Haskin, L. A. (1973). Experimental studies of the distribution
4
5 663 of rare earths as trace elements among silicate minerals and liquids and water. *Geochimica et*
6
7 664 *Cosmochimica Acta* **37**, 1499–1512.
- 8
9
10 665 Daczko, N. R., Clarke, G. L. & Klepeis, K. A. (2001a). Transformation of two-pyroxene
11
12 666 hornblende granulite to garnet granulite involving simultaneous melting and fracturing of the
13
14 667 lower crust, Fiordland, New Zealand. *Journal of Metamorphic Geology* **19**, 549–562.
- 15
16 668 Daczko, N. R., Clarke, G. L. & Klepeis, K. A. (2002a). Kyanite-paragonite-bearing
17
18 669 assemblages, northern Fiordland, New Zealand: rapid cooling of the lower crustal root to a
19
20 670 Cretaceous magmatic arc. *Journal of Metamorphic Geology* **20**, 887–902.
- 21
22
23 671 Daczko, N. R. & Halpin, J. A. (2009). Evidence for melt migration enhancing
24
25 672 recrystallization of metastable assemblages in mafic lower crust, Fiordland, New Zealand.
26
27 673 *Journal of Metamorphic Geology* **27**, 167–185.
- 28
29
30 674 Daczko, N. R., Klepeis, K. A. & Clarke, G. L. (2001b). Evidence of Early Cretaceous
31
32 675 collisional-style orogenesis in northern Fiordland, New Zealand and its effects on the
33
34 676 evolution of the lower crust. *Journal of Structural Geology* **23**, 693–713.
- 35
36 677 Daczko, N. R., Milan, L. & Halpin, J. (2009). Metastable persistence of pelitic metamorphic
37
38 678 assemblages at the root of a Cretaceous magmatic arc—Fiordland, New Zealand. *Journal of*
39
40 679 *Metamorphic Geology* **27**, 233–247.
- 41
42
43 680 Daczko, N. R., Piazzolo, S., Meek, U., Stuart, C. A. & Elliott, V. (2016). Hornblendite
44
45 681 delineates zones of mass transfer through the lower crust. *Scientific Reports* **6**, 31369.
- 46
47 682 Daczko, N. R., Stevenson, J. A., Clarke, G. L. & Klepeis, K. A. (2002b). Successive
48
49 683 hydration and dehydration of high-*P* mafic granofels involving clinopyroxene-kyanite
50
51 684 symplectites, Mt Daniel, Fiordland, New Zealand. *Journal of Metamorphic Geology* **20**, 669–
52
53 685 682.
- 54
55
56
57
58
59
60

- 1
2
3 686 Daines, M. J. & Kohlstedt, D. L. (1997). Influence of deformation on melt topology in
4
5 687 peridotites. *Journal of Geophysical Research: Solid Earth* **102**, 10257–10271.
6
7 688 Dalpé, C. & Baker, D. R. (2000). Experimental investigation of large-ion-lithophile-element-,
8
9 689 high-field-strength-element- and rare-earth-element-partitioning between calcic amphibole
10
11 690 and basaltic melt: the effects of pressure and oxygen fugacity. *Contributions to Mineralogy*
12
13 691 *and Petrology* **140**, 233–250.
14
15 692 Davidson, C., Schmid, S. M. & Hollister, L. S. (1994). Role of melt during deformation in the
16
17 693 deep crust. *Terra Nova* **6**, 133-142.
18
19 694 Davidson, J., Turner, S., Handley, H., Macpherson, C. & Dosseto, A. (2007). Amphibole
20
21 695 “sponge” in arc crust? *Geology* **35**, 787–790.
22
23 696 De Paoli, M. C., Clarke, G. L. & Daczko, N. R. (2012). Mineral equilibria modeling of the
24
25 697 granulite–eclogite transition: Effects of whole-rock composition on metamorphic facies type-
26
27 698 assemblages. *Journal of Petrology* **53**, 949–970.
28
29 699 De Paoli, M. C., Clarke, G. L., Klepeis, K. A., Allibone, A. H. & Turnbull, I. M. (2009). The
30
31 700 eclogite–granulite transition: Mafic and intermediate assemblages at Breaksea Sound, New
32
33 701 Zealand. *Journal of Petrology* **50**, 2307–2343.
34
35 702 El Korh, A., Schmidt, S. T., Ulianov, A. & Potel, S. (2009). Trace element partitioning in
36
37 703 HP–LT metamorphic assemblages during subduction-related metamorphism, Ile de Groix,
38
39 704 France: a detailed LA-ICPMS study. *Journal of Petrology* **50**, 1107–1148.
40
41 705 Esawi, E. K. (2004). AMPH-CLASS: An Excel spreadsheet for the classification and
42
43 706 nomenclature of amphiboles based on the 1997 recommendations of the International
44
45 707 Mineralogical Association. *Computers & Geosciences* **30**, 753–760.
46
47 708 Flynn, R. T. & Burnham, W. C. (1978). An experimental determination of rare earth partition
48
49 709 coefficients between a chloride containing vapor phase and silicate melts. *Geochimica et*
50
51 710 *Cosmochimica Acta* **42**, 685–701.
52
53
54
55
56
57
58
59
60

- 1
2
3 711 Frei, D., Liebscher, A., Franz, G. & Dulski, P. (2004). Trace element geochemistry of epidote
4
5 712 minerals. *Reviews in Mineralogy and Geochemistry* **56**, 553–605.
6
7 713 Frei, D., Liebscher, A., Wittenberg, A. & Shaw, C. S. J. (2003). Crystal chemical controls on
8
9 714 rare earth element partitioning between epidote-group minerals and melts: an experimental
10
11 715 and theoretical study. *Contributions to Mineralogy and Petrology* **146**, 192–204.
12
13 716 Gardner, R. L., Piazzolo, S. & Daczko, N. R. (2016). Shape of pinch and swell structures as a
14
15 717 viscosity indicator: Application to lower crustal polyphase rocks. *Journal of Structural*
16
17 718 *Geology* **88**, 32–45.
18
19 719 Green, T. H. (1982). Anatexis of mafic crust and high pressure crystallization of andesite.
20
21 720 *Andesites*, 465–487.
22
23 721 Griffin, W. L., Powell, W. J., Pearson, N. J. & O'Reilly, S. Y. (2008). GLITTER: data
24
25 722 reduction software for laser ablation ICP-MS. *Laser Ablation-ICP-MS in the earth sciences.*
26
27 723 *Mineralogical association of Canada short course series* **40**, 204–207.
28
29 724 Gromet, L. P. & Silver, L. T. (1983). Rare earth element distributions among minerals in a
30
31 725 granodiorite and their petrogenetic implications. *Geochimica et Cosmochimica Acta* **47**, 925–
32
33 726 939.
34
35 727 Hammarstrom, J. M. & Zen, E. (1986). Aluminum in hornblende; an empirical igneous
36
37 728 geobarometer. *American Mineralogist* **71**, 1297–1313.
38
39 729 Hollis, J. A., Clarke, G. L., Klepeis, K. A., Daczko, N. R. & Ireland, T. R. (2003).
40
41 730 Geochronology and geochemistry of high-pressure granulites of the Arthur River Complex,
42
43 731 Fiordland, New Zealand: Cretaceous magmatism and metamorphism on the palaeo-Pacific
44
45 732 Margin. *Journal of Metamorphic Geology* **21**, 299–313.
46
47 733 Hollis, J. A., Clarke, G. L., Klepeis, K. A., Daczko, N. R. & Ireland, T. R. (2004). The
48
49 734 regional significance of Cretaceous magmatism and metamorphism in Fiordland, New
50
51 735 Zealand, from U-Pb zircon geochronology. *Journal of Metamorphic Geology* **22**, 607-627.
52
53
54
55
56
57
58
59
60

- 1
2
3 736 Hollister, L. S., Grissom, G. C., Peters, E. K., Stowell, H. H. & Sisson, V. B. (1987).
4
5 737 Confirmation of the empirical correlation of Al in hornblende with pressure of solidification
6
7 738 of calc-alkaline plutons. *American Mineralogist* **72**, 231–239.
8
9 739 Holness, M. B. (2008). Decoding migmatite microstructures. In: Sawyer, E. W. & Brown, M.
10
11 740 (eds.) *Working with Migmatites*: Mineralogical Association of Canada, Short Course Volume
12
13 741 38, 57–76.
14
15 742 Holtzman, B. K., Groebner, N. J., Zimmerman, M. E., Ginsberg, S. B. & Kohlstedt, D. L.
16
17 743 (2003). Stress-driven melt segregation in partially molten rocks. *Geochemistry, Geophysics,*
18
19 744 *Geosystems* **4**, 8607.
20
21 745 Leake, B. E., Woolley, A. R., Arps, C. E. S., Birch, W. D., Gilbert, M. C., Grice, J. D.,
22
23 746 Hawthorne, F. C., Kato, A., Kisch, H. J., Krivovichev, V. G., Linthout, K., Laird, J.,
24
25 747 Mandarino, J. A., Maresch, W. V., Nickel, E. H., Rock, N. M. S., Schumacher, J. C., Smith,
26
27 748 D. C., Stephenson, N. C. N., Ungaretti, L., Whittaker, E. J. W. & Youzhi, G. (1997).
28
29 749 Nomenclature of amphiboles: Report of the Subcommittee on Amphiboles of the International
30
31 750 Mineralogical Association, Commission on New Minerals and Mineral Names. *European*
32
33 751 *Journal of Mineralogy* **35**, 219–246.
34
35 752 Leshner, C. E. (1994). Kinetics of Sr and Nd exchange in silicate liquids: Theory, experiments,
36
37 753 and applications to uphill diffusion, isotopic equilibration, and irreversible mixing of magmas.
38
39 754 *Journal of Geophysical Research: Solid Earth* **99**, 9585–9604.
40
41 755 Lundstrom, C., Gill, J., Williams, Q. & Perfit, M. (1995). Mantle melting and basalt
42
43 756 extraction by equilibrium porous flow. *Science* **270**, 1958–1961.
44
45 757 Mann, A. W. H. (1980). Diffusion in natural silicate melts: A critical review. In: Hargraves,
46
47 758 R. B. (ed.) *Physics of Magmatic Processes*. Princeton, New Jersey: Princeton University
48
49 759 Press, 385–418.
50
51
52
53
54
55
56
57
58
59
60

- 1
2
3 760 McDonough, W. F. & Sun, S. s. (1995). The composition of the Earth. *Chemical Geology*
4
5 761 **120**, 223–253.
6
7 762 Meek, U. (2015). An investigation of the origin of ultrabasic granofels, Fiordland, New
8
9 763 Zealand. Masters of Research, Macquarie University.
10
11 764 Middlemost, E. A. K. (1994). Naming materials in the magma/igneous rock system. *Earth-*
12
13 765 *Science Reviews* **37**, 215–224.
14
15
16 766 Milan, L. A., Daczko, N. R., Clarke, G. L. & Allibone, A. H. (2016). Complexity of in-situ
17
18 767 zircon U–Pb–Hf isotope systematics during arc magma genesis at the roots of a Cretaceous
19
20 768 arc, Fiordland, New Zealand. *Lithos* **264**, 296–314.
21
22
23 769 Mortimer, N., Tulloch, A. J., Spark, R. N., Walker, N. W., Ladley, E., Allibone, A. &
24
25 770 Kimbrough, D. L. (1999). Overview of the Median Batholith, New Zealand: a new
26
27 771 interpretation of the geology of the Median Tectonic Zone and adjacent rocks. *Journal of*
28
29 772 *African Earth Sciences* **29**, 257–268.
30
31
32 773 Mulrooney, D. & Rivers, T. (2005). Redistribution of the rare-earth elements among
33
34 774 coexisting minerals in metamafic rocks across the epidote-out isograd: An example from the
35
36 775 St. Anthony Complex, Northern Newfoundland, Canada. *The Canadian Mineralogist* **43**,
37
38 776 263–294.
39
40
41 777 Nicolas, A. (1986). A melt extraction model based on structural studies in mantle peridotites.
42
43 778 *Journal of Petrology* **27**, 999–1022.
44
45 779 O'Brien, P. J. & Rötzler, J. (2003). High-pressure granulites: formation, recovery of peak
46
47 780 conditions and implications for tectonics. *Journal of Metamorphic Geology* **21**, 3–20.
48
49 781 Otten, M. T. (1984). The origin of brown hornblende in the Artfjället gabbro and dolerites.
50
51 782 *Contributions to Mineralogy and Petrology* **86**, 189–199.
52
53
54 783 Paterson, D., de Jonge, M. D., Howard, D. L., Lewis, W., McKinlay, J., Starritt, A., Kusel,
55
56 784 M., Ryan, C. G., Kirkham, R., Moorhead, G. & Siddons, D. P. (2011). The X-ray
57
58
59
60

- 1
2
3 785 Fluorescence Microscopy Beamline at the Australian Synchrotron. *AIP Conference*
4
5 786 *Proceedings* **1365**, 219–222.
6
7 787 Pattison, D. R. M. (2003). Petrogenetic significance of orthopyroxene-free garnet +
8
9 788 clinopyroxene + plagioclase ± quartz-bearing metabasites with respect to the amphibolite and
10
11 789 granulite facies. *Journal of Metamorphic Geology* **21**, 21–34.
12
13 790 Pirard, C. & Hermann, J. (2015). Focused fluid transfer through the mantle above subduction
14
15 791 zones. *Geology* **43**, 915–918.
16
17 792 Plank, T. & Langmuir, C. H. (1993). Tracing trace elements from sediment input to volcanic
18
19 793 output at subduction zones. *Nature* **362**, 739–743.
20
21 794 Rampone, E., Piccardo, G., Vannucci, R., Bottazzi, P. & Zanetti, A. (1994). Melt
22
23 795 impregnation in ophiolitic peridotite: an ion microprobe study of clinopyroxene and
24
25 796 plagioclase. *Mineralogical Magazine* **58**, 756–757.
26
27 797 Rasband, W. S. (1997–2015). ImageJ. Bethesda, Maryland, USA, <http://imagej.nih.gov/ij/>: U.
28
29 798 S. National Institutes of Health.
30
31 799 Rosenberg, C. L. & Handy, M. R. (2000). Syntectonic melt pathways during simple shearing
32
33 800 of a partially molten rock analogue (Norcamphor-Benzamide). *Journal of Geophysical*
34
35 801 *Research: Solid Earth* **105**, 3135–3149.
36
37 802 Ryan, C. G. (2000). Quantitative trace element imaging using PIXE and the nuclear
38
39 803 microprobe. *International Journal of Imaging Systems and Technology* **11**, 219–230.
40
41 804 Ryan, C. G., Cousens, D. R., Sie, S. H., Griffin, W. L., Suter, G. F. & Clayton, E. (1990).
42
43 805 Quantitative pixe microanalysis of geological material using the CSIRO proton microprobe.
44
45 806 *Nuclear Instruments and Methods in Physics Research Section B: Beam Interactions with*
46
47 807 *Materials and Atoms* **47**, 55–71.
48
49 808 Ryan, C. G., Kirkham, R., Hough, R. M., Moorhead, G., Siddons, D. P., De Jonge, M. D.,
50
51 809 Paterson, D. J., De Geronimo, G., Howard, D. L. & Cleverley, J. S. (2010a). Elemental X-ray
52
53
54
55
56
57
58
59
60

1
2
3
4
5
6
7
8
9
10
11
12
13
14
15
16
17
18
19
20
21
22
23
24
25
26
27
28
29
30
31
32
33
34
35
36
37
38
39
40
41
42
43
44
45
46
47
48
49
50
51
52
53
54
55
56
57
58
59
60

810 imaging using the Maia detector array: the benefits and challenges of large solid-angle.
811 *Nuclear Instruments and Methods in Physics Research Section A: Accelerators,*
812 *Spectrometers, Detectors and Associated Equipment* **619**, 37–43.

813 Ryan, C. G., Siddons, D. P., Kirkham, R., Dunn, P. A., Kuczewski, A., Moorhead, G., De
814 Geronimo, G., Paterson, D. J., De Jonge, M. D. & Hough, R. M. (2010b). The new Maia
815 detector system: methods for high definition trace element imaging of natural material. *X-*
816 *RAY OPTICS AND MICROANALYSIS: Proceedings of the 20th International Congress.*
817 Karlsruhe, Germany, 9–17.

818 Sawyer, E. W. (1999). Criteria for the recognition of partial melting. *Physics and Chemistry*
819 *of the Earth, Part A: Solid Earth and Geodesy* **24**, 269–279.

820 Schröter, F. C., Stevenson, J. A., Daczko, N. R., Clarke, G. L., Pearson, N. J. & Klepeis, K.
821 A. (2004). Trace element partitioning during high-P partial melting and melt-rock interaction;
822 an example from northern Fiordland, New Zealand. *Journal of Metamorphic Geology* **22**,
823 443–457.

824 Smith, D. J. (2014). Clinopyroxene precursors to amphibole sponge in arc crust. *Nature*
825 *communications* **5**, 4329.

826 Smith, J. R., Piazzolo, S., Daczko, N. R. & Evans, L. (2015). The effect of pre-tectonic
827 reaction and annealing extent on behaviour during subsequent deformation: Insights from
828 paired shear zones in the lower crust of Fiordland, New Zealand. *Journal of Metamorphic*
829 *Geology* **33**, 557–577.

830 Spiegelman, M. & Elliott, T. (1993). Consequences of melt transport for uranium series
831 disequilibrium in young lavas. *Earth and Planetary Science Letters* **118**, 1–20.

832 Stevenson, J. A., Daczko, N. R., Clarke, G. L., Pearson, N. & Klepeis, K. A. (2005). Direct
833 observation of adakite melts generated in the lower continental crust, Fiordland, New
834 Zealand. *Terra Nova* **17**, 73–79.

- 1
2
3 835 Stowell, H., Parker, K. O., Gatewood, M., Tulloch, A. & Koenig, A. (2014). Temporal links
4
5 836 between pluton emplacement, garnet granulite metamorphism, partial melting and extensional
6
7 837 collapse in the lower crust of a Cretaceous magmatic arc, Fiordland, New Zealand. *Journal of*
8
9 838 *Metamorphic Geology* **32**, 151–175.
- 10
11 839 Stowell, H., Tulloch, A., Zuluaga, C. & Koenig, A. (2010). Timing and duration of garnet
12
13 840 granulite metamorphism in magmatic arc crust, Fiordland, New Zealand. *Chemical Geology*
14
15 841 **273**, 91–110.
- 16
17
18 842 Stuart, C. A., Daczko, N. R. & Piazzolo, S. (in press). Local partial melting of the lower crust
19
20 843 triggered by hydration through melt–rock interaction: an example from Fiordland, New
21
22 844 Zealand. *Journal of Metamorphic Geology*.
- 23
24
25 845 Stuart, C. A., Piazzolo, S. & Daczko, N. R. (2016). Mass transfer in the lower crust: Evidence
26
27 846 for incipient melt assisted flow along grain boundaries in the deep arc granulites of Fiordland,
28
29 847 New Zealand. *Geochemistry, Geophysics, Geosystems* **17**, 3733–3753.
- 30
31
32 848 Tetley, M. G. & Daczko, N. R. (2014). Virtual Petrographic Microscope: A multi-platform
33
34 849 education and research software tool to analyse rock thin-sections. *Australian Journal of*
35
36 850 *Earth Sciences* **61**, 631–637.
- 37
38
39 851 Tirone, M., Ganguly, J., Dohmen, R., Langenhorst, F., Hervig, R. & Becker, H.-W. (2005).
40
41 852 Rare earth diffusion kinetics in garnet: Experimental studies and applications. *Geochimica et*
42
43 853 *Cosmochimica Acta* **69**, 2385–2398.
- 44
45 854 Tulloch, A. J. & Kimbrough, D. L. (2003). Paired plutonic belts in convergent margins and
46
47 855 the development of high Sr/Y magmatism: Peninsular Ranges Batholith of Baja California
48
49 856 and Median Batholith of New Zealand. *Geological Society of America Special Papers* **374**,
50
51 857 275–295.
52
53
54
55
56
57
58
59
60

1
2
3 858 Van Orman, J. A., Grove, T. L. & Shimizu, N. (2001). Rare earth element diffusion in
4
5 859 diopside: Influence of temperature, pressure, and ionic radius, and an elastic model for
6
7 860 diffusion in silicates. *Contributions to Mineralogy and Petrology* **141**, 687–703.

8
9
10 861 Vernon, R. H. (2011). Microstructures of melt-bearing regional metamorphic rocks.
11
12 862 *Geological Society of America Memoirs* **207**, 1–11.

13
14 863 Wendlandt, R. F. & Harrison, W. J. (1979). Rare earth partitioning between immiscible
15
16 864 carbonate and silicate liquids and CO₂ vapor: Results and implications for the formation of
17
18 865 light rare earth-enriched rocks. *Contributions to Mineralogy and Petrology* **69**, 409–419.

19
20
21 866 White, R. W., Pomroy, N. E. & Powell, R. (2005). An in situ metatexite–diatexite transition
22
23 867 in upper amphibolite facies rocks from Broken Hill, Australia. *Journal of Metamorphic*
24
25 868 *Geology* **23**, 579–602.

26
27 869 Whitney, D. L. & Evans, B. W. (2010). Abbreviations for names of rock-forming minerals.
28
29 870 *American Mineralogist* **95**, 185–187.

30
31
32 871 **FIGURE CAPTIONS**

33
34
35 872 **Fig. 1:** Styles of melt rock interaction, showing from left to right: typical field relationships
36
37 873 including insets of a schematic cross section of the Pembroke Granulite showing relative scale
38
39 874 of each melt flux style; outcrop appearance; and microstructures of modified rock types (scale
40
41 875 bars 1000 μm), including insets of BSE images of microstructures indicative of the former
42
43 876 presence of melt. Mineral abbreviations follow the scheme proposed by Whitney and Evans
44
45 877 (2010). **a-c:** Style 1; **d-f:** Style 2, **g-i:** Style 3, **j-l:** Style 4.

46
47
48
49 878 **Fig. 2:** Whole rock composition of melt–rock interaction styles. **a:** TAS classification
50
51 879 diagram. **b:** Aluminium Harker diagram. **c:** Magnesium Harker diagram. **d:** SiO₂ plotted
52
53 880 against Sr/Y. **e:** Chondrite normalised REE ratios for Styles 1 and 2. **f:** Chondrite normalised
54
55 881 REE patterns for Style 4. Grey field is range of REE content in Styles 1 and 2.

1
2
3 882 **Fig. 3:** Mineral major element composition. **a:** A-site occupancy in amphiboles. **b:** Ti
4
5 883 (c.p.f.u.) in amphiboles. **c:** Garnet ternary classification diagram. **d:** Pistacite content in
6
7 884 clinozoisite.

8
9
10 885 **Fig. 4:** Range of Sr zoning in plagioclase. Note different Sr scales for each map. Mineral
11
12 886 abbreviations follow the scheme proposed by Whitney and Evans (2010). **a:** Style 1, field of
13
14 887 view (FOV) = 18 mm across. **b:** Style 2, FOV = 21.5 mm across. **c:** Style 3, FOV = 20 mm
15
16 888 across.

17
18
19 889 **Fig. 5:** Rare earth element profiles for amphibole, garnet and clinozoisite in the protolith, S_1 ,
20
21 890 and each melt–rock interaction style.

22
23
24 891 **Fig. 6:** Calculated P–T conditions for S_1 and each melt–rock interaction style. Inset:
25
26 892 schematic P–T diagram showing position of solidus, liquidus and plagioclase-out line relative
27
28 893 to the melt flux style conditions.

29
30
31
32 894 **Fig. 7:** Igneous and metamorphic signatures of mineral REE patterns. **a:** Published values for
33
34 895 igneous and metamorphic clinozoisite/epidote. Data from Gromet and Silver (1983), and El
35
36 896 Korh et al. (2009). **b:** Average REE patterns for clinozoisite from each melt–rock interaction
37
38 897 style. **c:** Published values for igneous and metamorphic amphibole. Data from Dalpé and
39
40 898 Baker (2000) and El Korh et al. (2009). **d:** Average REE patterns for amphibole from S_1 and
41
42 899 each melt–rock interaction style.
43
44
45
46
47
48
49
50
51
52
53
54
55
56
57
58
59
60

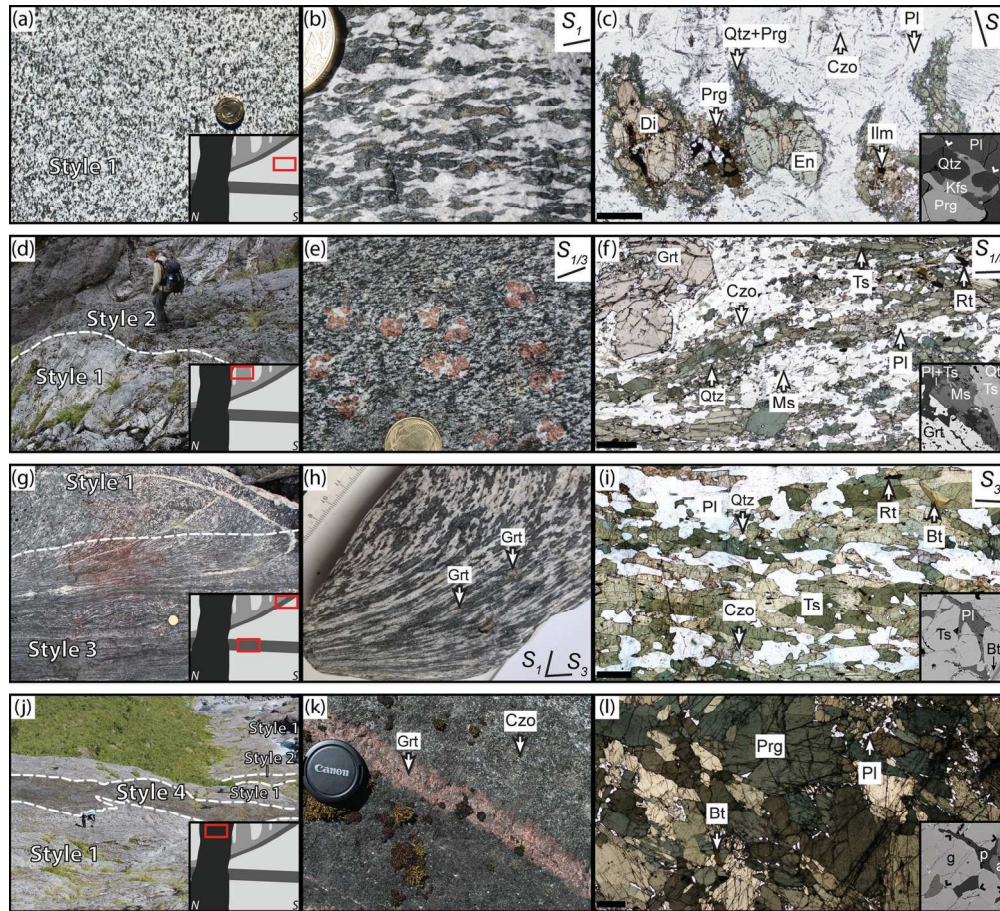


Fig. 1: Styles of melt rock interaction, showing from left to right: typical field relationships including insets of a schematic cross section of the Pembroke Granulite showing relative scale of each melt flux style; outcrop appearance; and microstructures of modified rock types (scale bars 1000 μm), including insets of BSE images of microstructures indicative of the former presence of melt. Mineral abbreviations follow the scheme proposed by Whitney and Evans (2010). a-c: Style 1; d-f: Style 2, g-i: Style 3, j-l: Style 4.

Fig. 1

149x135mm (300 x 300 DPI)

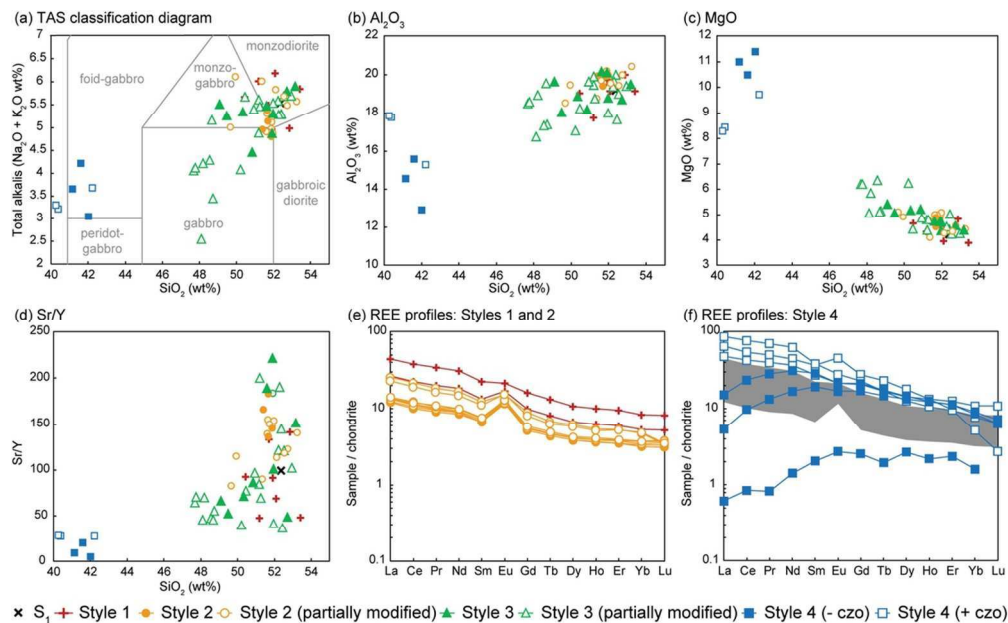


Fig. 2: Whole rock composition of melt-rock interaction styles. a: TAS classification diagram. b: Aluminium Harker diagram. c: Magnesium Harker diagram. d: SiO₂ plotted against Sr/Y. e: Chondrite normalised REE ratios for Styles 1 and 2. f: Chondrite normalised REE patterns for Style 4. Grey field is range of REE content in Styles 1 and 2.

Fig. 2
101x62mm (300 x 300 DPI)

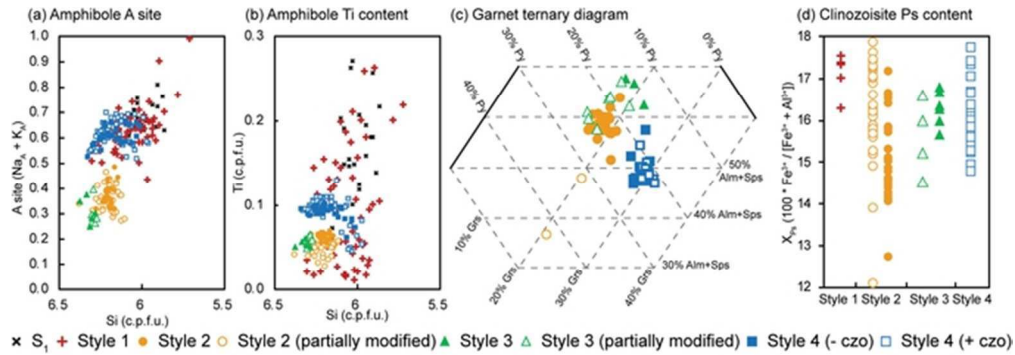


Fig. 3: Mineral major element composition. a: A-site occupancy in amphiboles. b: Ti (c.p.f.u.) in amphiboles. c: Garnet ternary classification diagram. d: Pistacite content in clinozoisite.

Fig. 3

57x20mm (300 x 300 DPI)

Peer Review

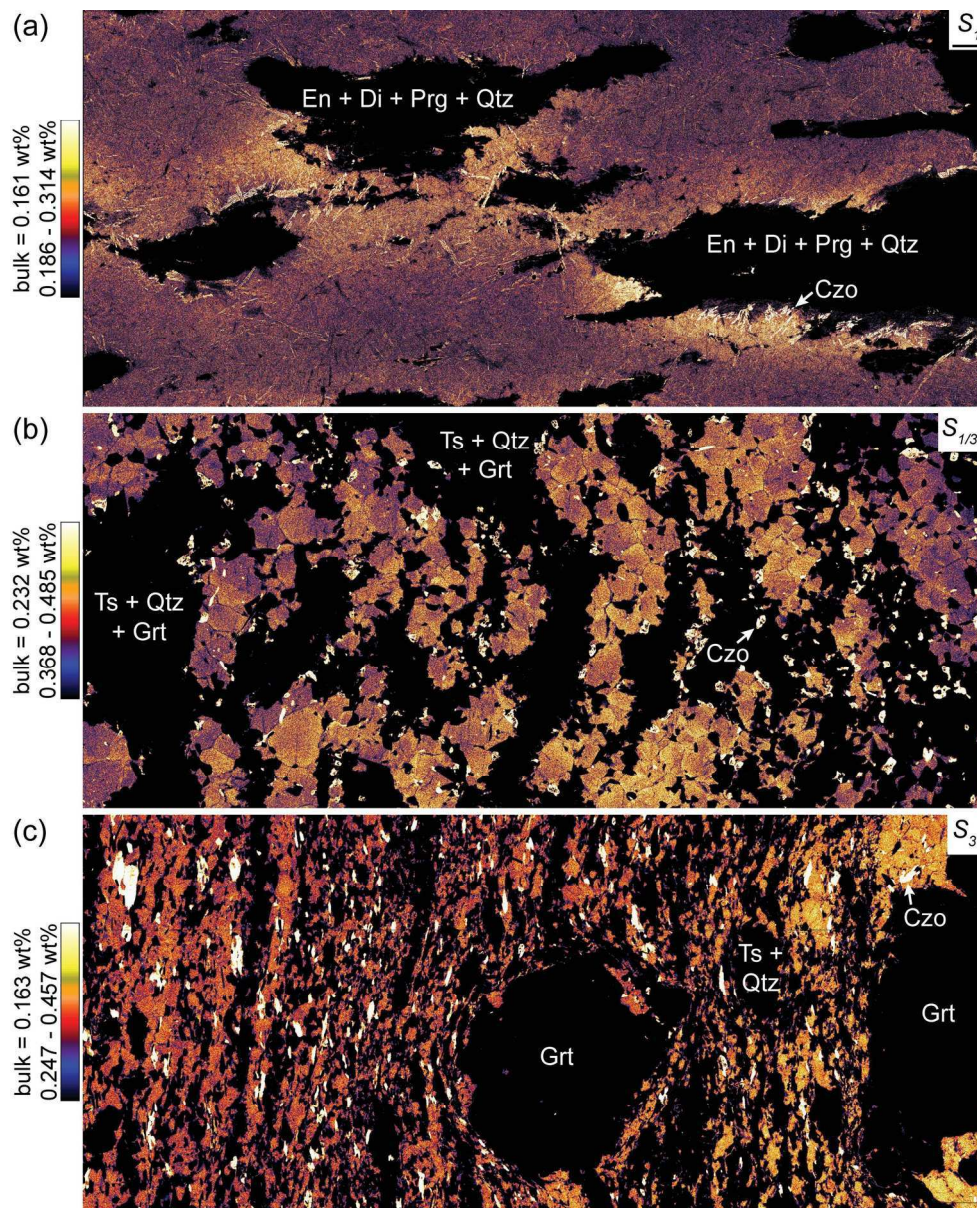


Fig. 4: Range of Sr zonation in plagioclase. Note different Sr scales for each map. Mineral abbreviations follow the scheme proposed by Whitney and Evans (2010). a: Style 1, field of view (FOV) = 18 mm across. b: Style 2, FOV = 21.5 mm across. c: Style 3, FOV = 20 mm across.

Fig. 4

173x213mm (300 x 300 DPI)

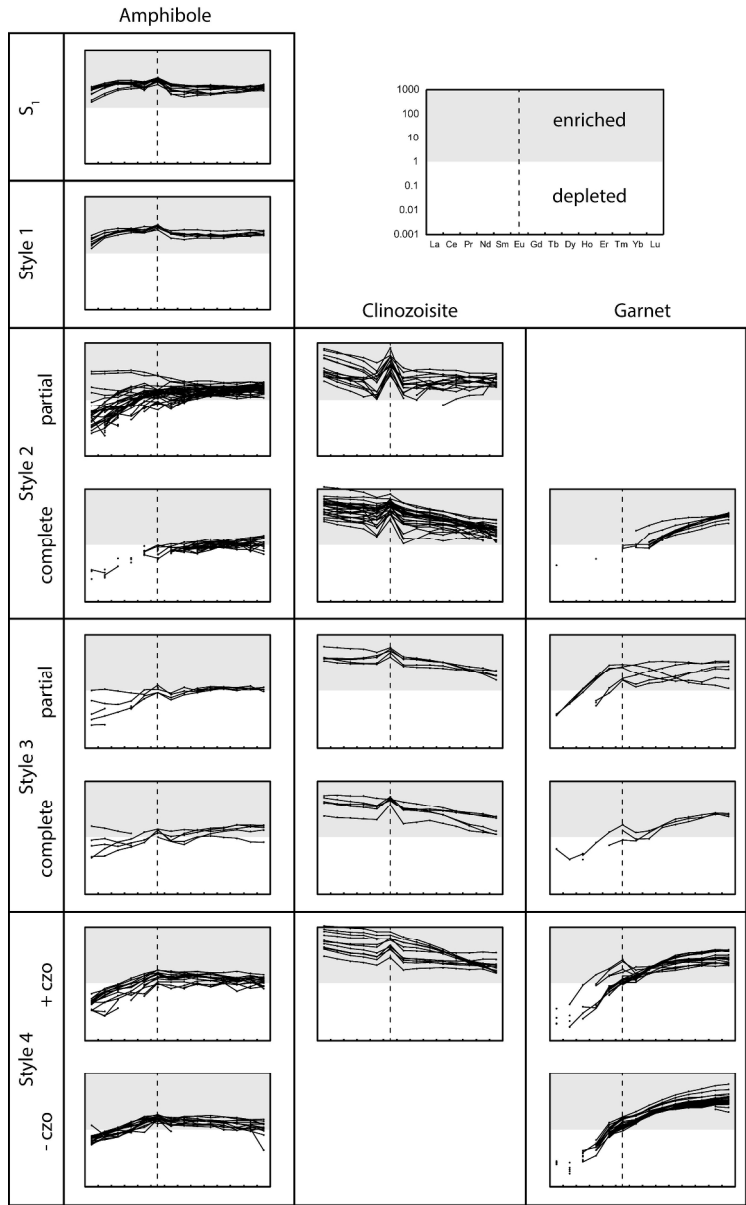


Fig. 5: Rare earth element profiles for amphibole, garnet and clinozoisite in the protolith, S₁, and each melt-rock interaction style.

Fig. 5

203x330mm (300 x 300 DPI)

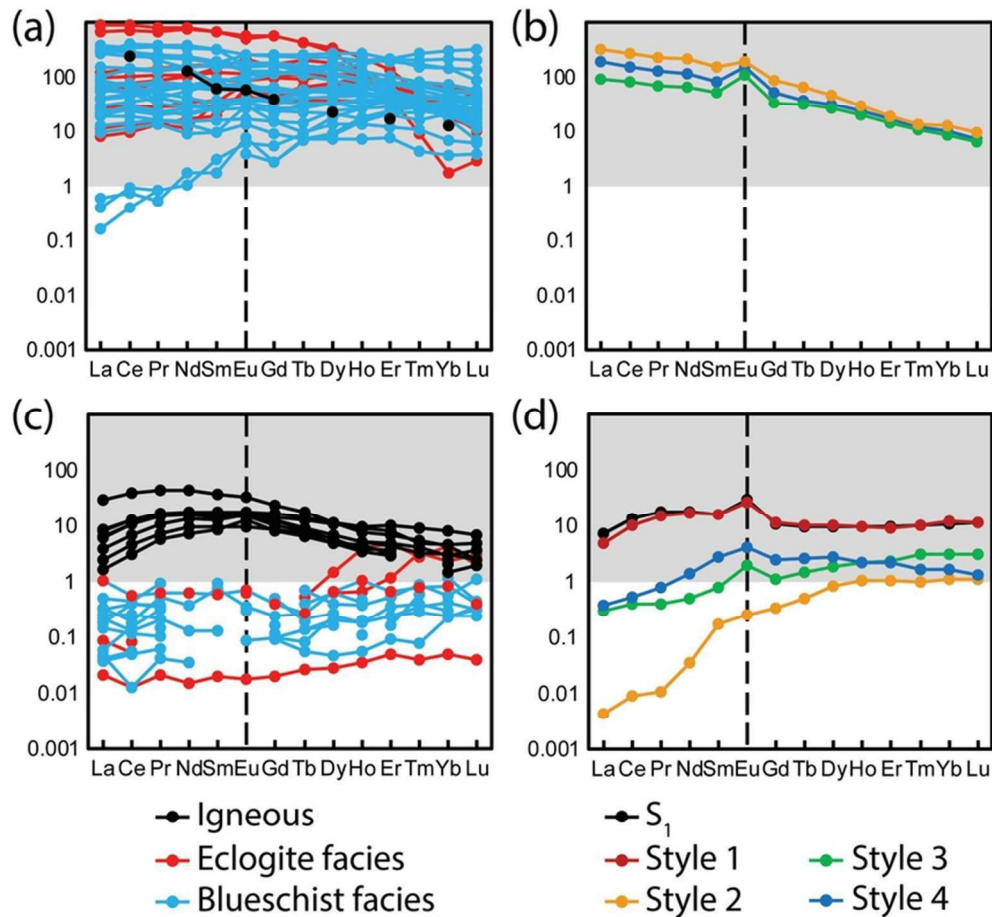
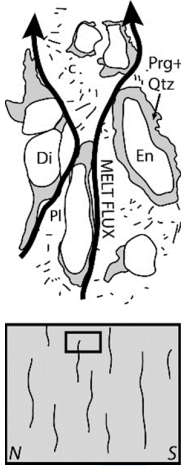
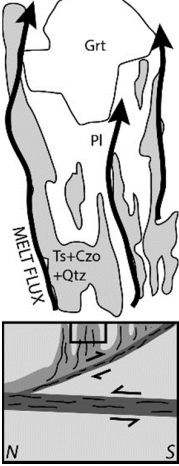
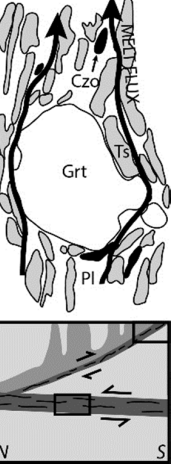
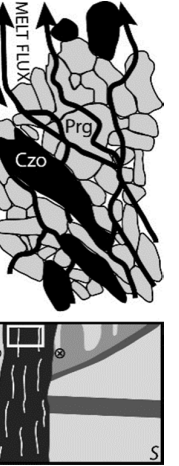


Fig. 7: Igneous and metamorphic signatures of mineral REE patterns. a: Published values for igneous and metamorphic clinzoisite/epidote. Data from Gromet and Silver (1983), and El Korh et al. (2009). b: Average REE patterns for clinzoisite from each melt-rock interaction style. c: Published values for igneous and metamorphic amphibole. Data from Dalpé and Baker (2000) and El Korh et al. (2009). d: Average REE patterns for amphibole from S₁ and each melt-rock interaction style.

Fig. 7

73x67mm (300 x 300 DPI)

Table 1: Summary of characteristics of melt flux styles in the Pembroke Granulite.				
Melt flux style	Style 1	Style 2	Style 3	Style 4
Sketch				
Interpreted process	Pervasive melt migration along grain boundaries at a kilometre scale.	Localised melt migration along grain boundaries within 10–20 m wide channels.	Localised melt migration along grain boundaries within active deforming shear zones (0.1–10m wide).	Localised melt migration along grain boundaries within an actively deforming shear zone (30–40m wide).
Key features	Melt–rock interaction is hydrating, with little to no change observed in bulk composition. Melt is pseudomorphed by plagioclase, K-feldspar, and quartz.	Melt–rock interaction is hydrating, with little to no change observed in bulk composition. Melt is pseudomorphed by quartz, plagioclase, amphibole, and K-feldspar.	Melt–rock reaction is hydration, with little to no change observed in bulk rock composition. Melt is pseudomorphed by quartz, plagioclase, K-feldspar, clinzoisite, and clinopyroxene.	Melt–rock interaction is hydrating and reactive, where significant changes to bulk composition. Melt is pseudomorphed by plagioclase, biotite, and garnet.
Relative timing	Post-S ₁ , pre-D ₂	Pre/syn-D ₃	Syn-D ₃	Syn/post-D ₃
P–T conditions	630–710°C, 8.8–12.4 kbar	Not calculated, above solidus	~675°C, 14 kbar	696–720°C, 9–10 kbar
Recrystallisation regime	Static	Static	Dynamic	Dynamic
Reaction	En + Di + Pl + melt -> Prg + Pl ± Czo + melt	En + Di + Pl + melt -> Ts + Czo + Pl + Grt + melt	minerals from all earlier rock types + melt -> Ts + Pl + Grt + Czo + melt	minerals from all earlier rock types + melt -> Prg + Grt + melt ± Czo
Relative cumulate flux at an outcrop scale	Very small	Small-intermediate	Intermediate	High
References	Stuart et al 2016	Stuart et al (in press)	Daczko et al 2001b	Daczko et al 2016; Meek 2015